Short-Range Correlations Studies in Nuclei via the A(p,2pN) Reaction with HADES

List of organizations and participants:
Germany: TUD, GSI, HADES and R^{3}B collaborations at GSI
Israel: Tel Aviv University
USA: MIT

Spokespersons for the SRC part of the proposal:
Or Hen (MIT), Eli Piasetzky (TAU)

Coordinators:
Romain Holzmann (GSI and Frankfurt University)
Jerzy Pietraszko (GSI)
Georgios Laskaris (MIT and TAU)

Abstract

In the last decade, experimental studies of short-range correlations (SRC) in nuclei yielded results with wide ranging implications for various aspects of nuclear, astro- and particle physics, relating to the short-range tensor and scalar parts of the nucleon-nucleon interaction, structure function modification and the EMC effect, neutrino-nucleus interactions and analysis of neutrino oscillation experiments, the nuclear symmetry energy, the structure and cooling mechanisms of neutron stars and more.

The main technological advance that made these studies possible was the growing availability of continuous, high-intensity, few-GeV proton (EVA-BNL) and electron (JLab) beams, which allowed performing hard-knockout reactions with large sensitivity to SRC pairs in nuclei. However, exclusive SRC studies have so far been statistically limited, with typical experiments measuring tens to hundreds of events.

We propose here to utilize the large acceptance of the HADES spectrometer and the high intensity of the SIS18 proton beam at incident energies of 4.5 GeV to perform an exclusive SRC studies using the A(p,2pN) reaction with thousands of SRC events.

The main goals of this measurement are to:

(1) Study the details of the short-range part of the nucleon-nucleon interaction, in particular the *transition from tensor dominance to the scalar repulsive core*.

(2) Map the transition from the mean field to the SRC dominated domain in the nuclear momentum distribution (*first observation of the nuclear Migdal jump*).

(3) Study the breakdown of reaction mechanism factorization at low energies as *preparation for SRC studies in short-lived nuclei using inverse kinematics at FAIR*.

(4) Measure the A-dependence of SRC pair abundance and properties in order to *deduce the quantum numbers of 2N-SRCs in nuclei*.

(5) *Study the three-nucleon force* by searching for three-nucleon short-range correlations (3N-SRC) in exclusive A(p,2p2N) reactions.

We propose to perform the SRC measurements at HADES in two stages. The first measurement of SRCs will run in parallel to a dedicated di-lepton measurement, using the SIS18 4.5 GeV proton beam in a fixed target mode and will be able to measure A(p,ppn) and A(p,ppnn) reactions involving only recoil neutrons. For the future SRC measurements, we propose to have a dedicated run using the SIS18 4.5 GeV proton beam in a fixed target mode that will be able to measure both recoil neutrons and protons, covering A(p,ppn) and A(p,ppp) reactions as well as possible 3N-SRC. To measure the recoil protons during the dedicated run, the RICH detector – that is part of the HADES spectrometer – should be removed. The HADES spectrometer will be used to measure the two leading protons in a quasi-elastic 90^{o} c.m. scattering topology and a large-acceptance REcoil Nucleon Detector (REND), composed of part of the NeuLAND detector and two smaller side walls, will be used for detecting recoil protons and neutrons at backward angles. Possible target nuclides that can be used in the experiment are: ^{12}C, ^{28}Si, ^{40,48}Ca, ^{56}Fe, ^{107}Ag, ^{112}Sn, ^{124}Sn and ^{208}Pb.

Content

1. Introduction

> "What holds the nucleus of the atom together? In the past quarter century physicists have devoted a huge amount of experimentation and mental labor to this problem – probably more man-hours than have been given to any other scientific question in the history of mankind." - **Hans Bethe, Scientific American 1953**.

> "However, the nuclear force is the residue of the much stronger, non-perturbative QCD force between quarks, and the fundamental nature of the short distance repulsion is not well understood in either picture" – **Physics Opportunities with the 12 GeV Upgrade at Jefferson Lab, August 2012**.

The stability of atomic nuclei is the result of a delicate balance between a long-range attraction that binds the nucleons together and a short-range repulsion that prevent their collapse. Understanding the nature of these different parts of the nucleon-nucleon (NN) interaction and the resulting structure of nuclei and nuclear matter is a long-standing challenge of both theoretical and experimental nuclear physics.

The simultaneous development of high-energy, high-luminosity accelerators on one hand and QCD and Effective Field Theories (EFT) on the other helped yield powerful insight into the long-range part of the NN-interaction. However, our understanding of the short-range (repulsive) part of the NN-interaction, as well as its effect on the structure of nuclei and nuclear matter, is still lacking.

The Short-Range Correlations (SRC) studies program at Brookhaven National Lab (BNL) and later at Jefferson-Lab (JLab) – where it was an important part of the JLab 6 GeV science program – helped uncover valuable information on the short-range structure of nuclei [1-10]. This program had a series of inclusive (e,e') [6-8] and exclusive (e,e'pN) [1-5] measurements on a variety of nuclei. The results of these measurements conclusively showed the existence of both np and pp two-nucleon (2N) SRC pairs in nuclei and studied some of their main characteristics, such as:

(1) The relative number of 2N-SRC pairs in different nuclei [9],
(2) The missing momentum dependence of the np/pp ratio [1-4],
(3) The fraction of np and pp SRC pairs out of all high-momentum protons [4,11],
(4) The c.m. motion of 2N-SRC pairs and its A-dependence [10].

These results have wide ranging implications for many aspects of nuclear, astro-, particle, and atomic physics. These include the importance of the short-range tensor part of the NN-interaction [12-14], mapping the transition to the repulsive (scalar) core [3], the origin of the EMC effect [15-18], the nature of cold, dense nuclear matter [1,19], the value of the nuclear symmetry energy at supra-nuclear densities [20], nuclear effects in neutrino-nucleus scattering and their effect on extraction of oscillation parameters [21,22], the effect of correlations on imbalanced two-component interacting Fermi systems [23] and more.

The first generation of exclusive, high-energy, large momentum transfer SRC studies was done at BNL using a 6 – 9 GeV/c medium-intensity proton beam, the EVA spectrometer, and a relatively small-acceptance recoil-neutron detector [1,24,25]. While this measurement allowed for the first direct observation of the breakup of np-SRC pairs, the event sample was limited to only ~30 ^{12}C(p,2pn) events. Follow-up measurements, using electron beams at JLab, allowed for a simultaneous direct observation pp-SRC and np-SRC pairs, and extended the measurements to various target nuclei (^{4}He, ^{12}C, ^{27}Al, ^{56}Fe, and ^{208}Pb) [1-4]. However, these were also statistically limited to between tens to hundreds of A(e,e'pp) and A(e,e'pn) events. This limitation resulted from the low signal rate and small signal-to-background ratio at the electron-beam kinematics required for probing SRCs (mainly due to the lower electron-proton cross-section at the relevant kinematics). The background rate also prevented the exclusive study of Three-Nucleon correlations (3N-SRCs).

For the proposed HADES measurement, we take a conservative approach and plan to execute the measurement in two stages. The first-stage SRC measurement will take place in parallel to a di-lepton run using the SIS18 4.5 GeV proton beam in a fixed target mode. This experiment will be the first SRC experiment with a dedicated trigger using the HADES spectrometer, and quality checks of the acquired data will be necessary. In this first measurement, we will be able to measure A(p,ppn) and A(p,ppnn) reactions that involve the detection of backward going recoil neutrons only. For the second stage of SRC measurements, we propose to have a dedicated run using the SIS18 4.5 GeV proton beam in a fixed target mode being able to detect backward going neutrons and protons in order to measure both A(p,ppn) and A(p,ppp) reactions as well as possible 3N-SRCs. To measure the recoil protons during this dedicated run, the RICH detector – which is part of HADES spectrometer – should be removed.

Using of the SIS18 proton beam at 4.5 GeV, combined with the large acceptance of the HADES spectrometer and a dedicated REcoil Nucleon Detector (REND), one can utilize the large proton-proton cross-sections to measure pp- and np-SRC pairs, and possible 3N-SRC over a large kinematical regime with **large statistics**.

The drastic increase in statistics expected with a proton beam will open a window to:

1. Study the details of the short-range part of the nucleon-nucleon interaction, in particular the *transition from tensor dominance to scalar repulsive core*.
2. Map the transition from the mean field to the SRC dominated domain in the nuclear momentum distribution (*first observation of the nuclear Migdal jump*).
3. Study the breakdown of reaction mechanism factorization at low energies as *preparation for SRC studies in short-lived nuclei using inverse kinematics at FAIR*.
4. Measure the A-dependence of SRC pair abundance and properties in order to *deduce the quantum numbers of 2N-SRCs in nuclei*.

5. *Study the three-nucleon force* by exploring the 3N-SRC in exclusive A(p,2p2N) reactions.

The experiment proposed here will use the SIS18 proton beam at the energies of 4.5 GeV in the HADES experimental hall to address these topics by performing a high-statistics measurement of the A(p,2pN) and A(p,2p2N) reactions, and 3N-SRC reactions on the possible target nuclides ^{12}C, ^{28}Si, ^{40,48}Ca, ^{56}Fe, ^{107}Ag, ^{112}Sn, ^{124}Sn and ^{208}Pb.

2. Scientific Background

The existence, nature, and prevalence of 2N-SRCs in nuclei raise fundamental issues in modern nuclear physics (see popular summary in ref [26] and reviews in [27-29]). Understanding the nature and different characteristics of these multi-nucleon SRCs are vital for the study of:

1. The possible difference between the structure of bound and free nucleons (i.e. nucleon structure modification in the nuclear medium and the EMC effect),
2. The strong short-range force between nucleons (tensor, repulsive core, and 3N forces),
3. High-momentum components of the nuclear wave function,
4. Cold, dense, symmetric and asymmetric nuclear matter (from deuteron to neutron stars),
5. Nuclear effects in neutrino-nucleus interactions.

SRCs in nuclei have been actively investigated for over three decades. However, experimental studies of the microscopic structure of SRCs were very restricted, due to the use of moderate momentum-transfer kinematics in which it is difficult to resolve SRCs. During the past 15 years, SRC measurements were carried out via high-energy proton-nucleus reactions at the Brookhaven National Laboratory EVA experiment (EVA/BNL) [1,24,25], and electron-nucleus scattering reactions at the Thomas Jefferson National Accelerator Facility (JLab) [1-8]. These measurements have identified two-nucleon short-range correlations, studied their structure, and related them to the underlying basic short-range nucleon-nucleon (NN) interaction and to the EMC effect.

This proposal utilizes the combination of the high-intensity proton beam of SIS18 at incident energies of 4.5 GeV and the large acceptance of the HADES spectrometer, to extend the study of SRCs beyond what was possible with very low event rates at EVA/BNL.

2.1. Previous Measurements

2.1.1. Inclusive (e,e') measurements

Large-Q^2 inclusive (e,e') measurements, done in Halls B and C, observed scaling in cross section ratios for nuclei relative to deuterium at large values of x_B (= Q^2 / $2m_N\omega$, where m_N the proton mass, and ω the energy transfer). This scaling was observed in the region of $Q^2 > 1.4$ GeV^2/c^2 and $1.4 < x_B < 2$, where the reaction is

dominated by scattering off of nucleons in the nucleus with high initial momentum (see Fig. 2), and confirmed earlier observations of scaling for nucleus-to-deuteron cross section ratios from SLAC [18]. This scaling behavior indicates that the electron is probing high-momentum nucleons coming from local sources in the nuclear wave function (i.e., SRCs). These SRCs are sensitive to the short-range forces between two close nucleons and only weakly depend on the non-correlated residual nucleus.

The measured onset of the x_B scaling was used to extract the onset region in momentum where the wave function is dominated by such SRCs. The scaling parameter, commonly referred to as $a_2(A/d)$, can be used to determine the overall probability for a nucleon to be part of such an SRCs state. In ^{12}C the probability to be a member of a two-nucleon SRC state [proton-proton (pp), neutron-proton (np), or neutron-neutron (np)] was estimated to be (20±5)% [6-8].

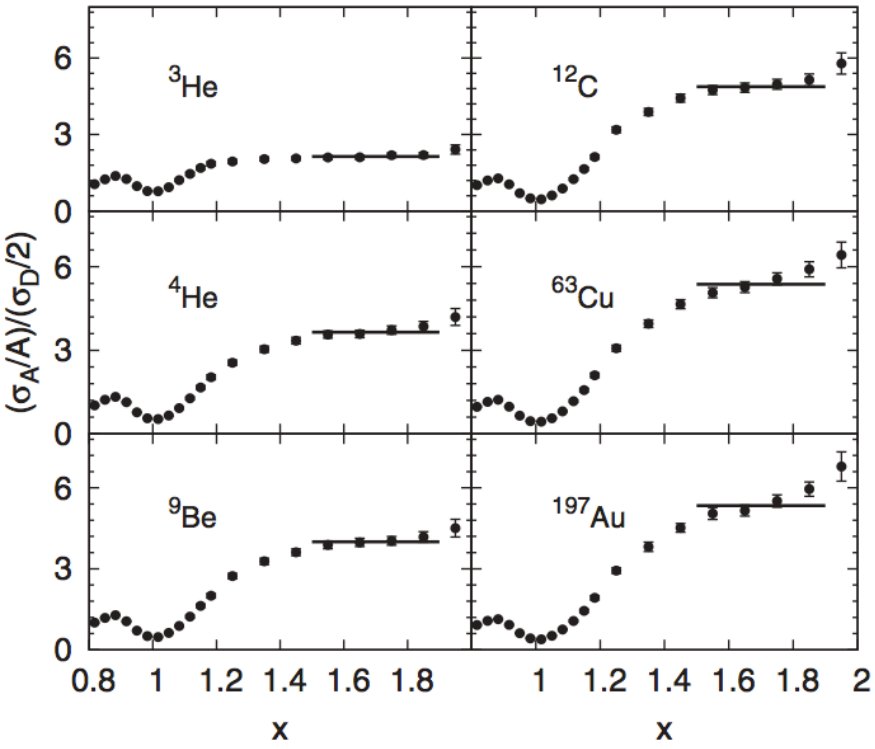

Fig. 2: The inclusive (e,e') cross section ratios for nuclei relative to deuterium as a function of x_B for $<Q^2>=2.7$ GeV/c^2. The solid lines indicate the 2N-SRC scaling regions. See Refs. [6-8].

2.1.2. Exclusive ^{12}C(p,2pn) measurements

The hypothesis that inclusive (e,e') reactions at large x_B probe high momentum bound nucleons from 2N-SRC pairs has been supported by high-energy, large momentum transfer ^{12}C(p,2pn) measurements at EVA/BNL [1,24,25]. These triple coincidence measurements directly observed the existence of np-SRC pairs

(Fig. 3). Analyses of these data show that in ^{12}C, 92_{-18}^{+8} % of all high-momentum nucleons are part of 2N-SRC pairs and, furthermore, that these pairs are predominantly np in character [25]. The uncertainties in the EVA/BNL data are large, so it was only possible to set an upper limit of about 13% on the pp-SRC/np-SRC ratio in carbon.

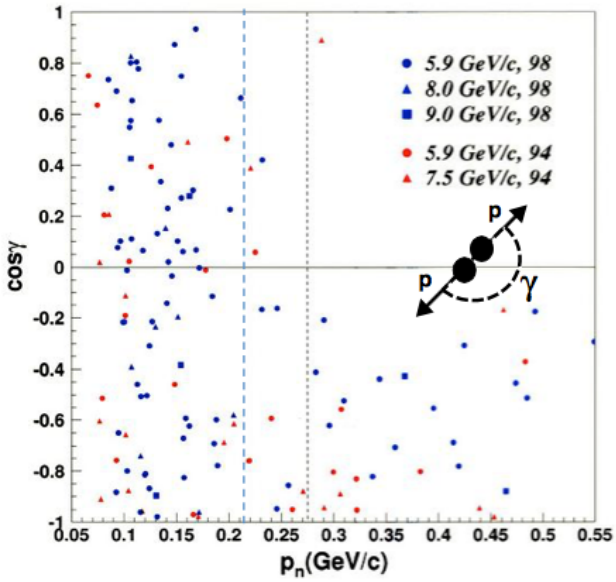

Fig. 3: The correlation between the neutron momentum p_n and its direction γ relative to the initial momentum of the struck proton (Migdal jump). Data labeled by 94 and 98 are from Ref. [24,30] respectively. The momenta are the beam momenta. The dashed vertical line corresponds to k_F = 220 MeV/c.

2.1.3. Exclusive A(e,e'pN) measurement on ^{4}He and ^{12}C

A further study of pp-SRC pairs and the dependence of the np/pp SRC pair ratio on missing momentum was carried out in subsequent measurements (E01-015 and E07-006) at Hall-A [1,3,4]. In these experiments, a simultaneous measurement of the triple coincidence A(e,e'pp) and A(e,e'pn) reactions as well as the double coincidence A(e,e'p) reaction at large Q^2, $x_B > 1$ kinematics was performed.

The first measurement was performed using a ^{12}C target and covered an A(e,e'p) missing (initial) momentum range of 300–600 MeV/c. The second (follow-up) measurement was performed using a ^{4}He target and covered a missing momentum range of 450–850 MeV/c. The goal of the second experiment was to study pairs that are even closer to each other, probing distance scales that are dominated by the nucleon-nucleon repulsive hard core. This hard core, which is essentially unexplored experimentally, is hypothesized to be of a scalar form.

Fig. 4 shows the characteristics of the measured ^{4}He(e,pN) events. The figure shows the opening angle between the missing-momentum of the leading proton and the recoil neutron. The insert shows the missing mass spectra of the residual A-2 system for both ^{4}He(e,e'pp) and ^{4}He(e,e'pn) events. The angular correlation exhibits a clear back-to-back peak above the background. The observed missing

mass spectra are consistent with a two-nucleon residual system with low excitation energy. These distributions support the picture of a Quasi-Elastic (QE) knockout of a correlated pair.

Fig. 5 and 6 shows combined results of both the ^{12}C and ^{4}He measurements. We divide the discussion of these results into two missing momentum regions: 300 – 600 MeV/c and 600–850 MeV/c:

1. At a missing momentum range of 300–600 MeV/c, these results from JLab $^{12}C(e,e'pN)$ measurements, combined with those of the inclusive A(e,e') cross-section ratios and the EVA/BNL $^{12}C(p,2pn)$ measurement, show that:
    1. Nucleons in 2N-SRC are 20 – 25% of all nucleons in medium and heavy nuclei. These pairs dominate the nuclear wave function above the Fermi momentum ($k > k_F$).
    2. np-SRC pairs dominate over pp-SRC pairs by a factor of ~20.

The startlingly large ratio of np-SRC/pp-SRC at the missing momentum range of 300–600 MeV/c prompted new theoretical work by three nuclear theory groups [22-24]. These theoretical studies showed that the measured ratio is a strong indication of the NN tensor force at the small nucleon separations (large relative momenta) studied. The theoretical conclusions are in agreement with earlier studies of nucleon momentum distribution n(k) for large momenta that also indicated dominance of tensor correlations.

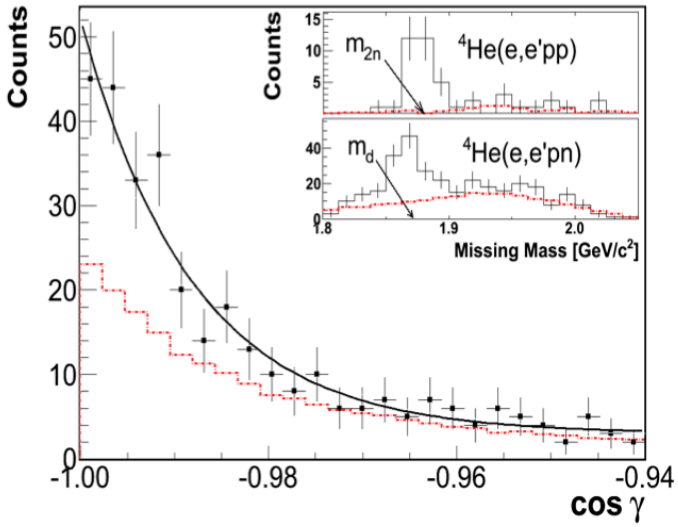

Fig. 4: The distribution of the cosine of the opening angle γ between the missing-momentum and recoil nucleon momentum for the $^{4}He(e,e'pn)$. The solid curve is a simulation of scattering off a moving pair with a CM momentum having a width of 100 MeV/c. The inserts show the missing-mass distributions. In both the main figure and the inserts, the data are shown with no random background subtraction. The random background is shown with red (online), dotted curves.

2. At a missing momentum range of 600–850 MeV/c, the number of np-SRC pairs is reduced while the number of pp-SRC pairs remains constant. This is understood as evidence for the contribution of the scalar (repulsive) part of the

NN-interaction. Fig. 5 also shows a comparison of the ^{4}He results with recent many-body Variational Monte-Carlo (VMC) calculation of the two-body nuclear momentum distributions.

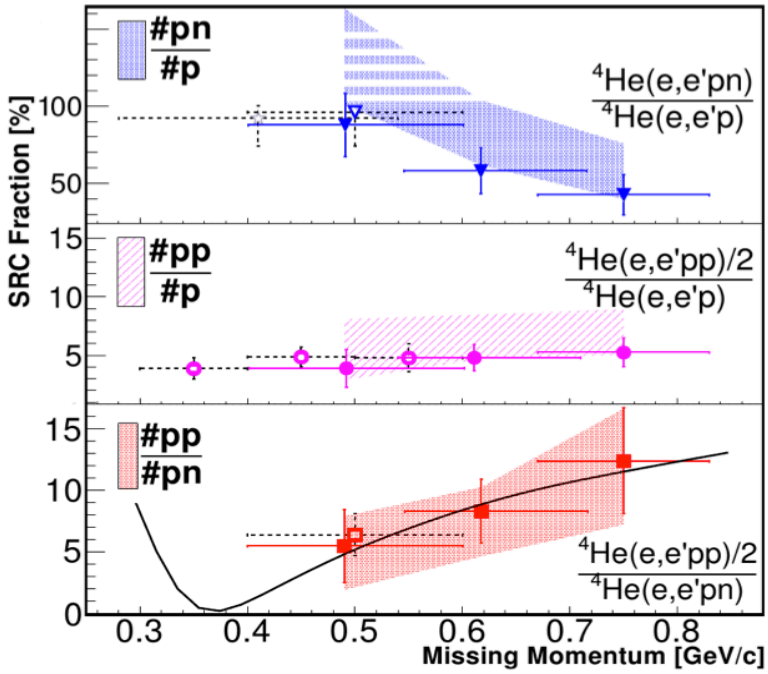

Fig. 5: Lower panel: The measured ratio ^{4}He(e,e'pp)/^{4}He(e,e'pn) shown as solid symbols, as a function of the ^{4}He(e,e'p) missing momentum. Each point is the result of a different setting of the detectors. The bands represent the data corrected for FSI to obtain the pair ratios. Also shown are VMC calculations pairs with weighted-average c.m. momentum assuming arbitrary angles between the CM and the relative momenta in the pair (solid black line). The middle panel shows the measured ^{4}He(e,e'pp)/ ^{4}He(e,e'p) and extracted #pp/#p ratios. The upper panel shows the measured ^{4}He(e, e'pn)/ ^{4}He(e, e'p) and extracted #pn/#p ratios. Ratios for ^{12}C are shown as empty symbols with dashed bars. The empty star in the upper panel is the BNL result for ^{12}C (p, 2pn)/ ^{12}C (p, 2p).

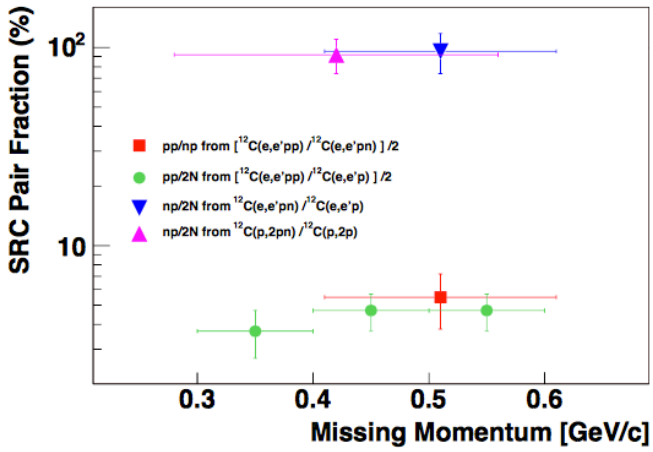

Fig. 6: The relative fraction of np and pp SRC pairs in ^{12}C as extracted from the JLab ^{12}C(e,e'pN) and BNL ^{12}C(p,2pn) measurements.

2.1.4. Exclusive A(e,e'pp) measurement on heavy, asymmetric, nuclei

Information on the dynamics of 2N-SRC pairs in heavier nuclei came from recent analysis of A(e,e'p) and A(e,e'pp) data on ^{12}C, ^{27}Al, ^{56}Fe, and ^{208}Pb targets, conducted as part of the Hall-B data-mining project [2]. The analysis focused on large-Q^2, $x_B > 1.2$, kinematics where the reaction is dominated by scattering off of 2N-SRC pairs. In these kinematics, the A(e,e'p) reaction is sensitive to both np-an pp-SRC pairs while the A(e,e'pp) reaction is sensitive to pp-SRC pairs alone. While this measurement was not directly sensitive to np-SRC pairs, the fact that very few of the A(e,e'p) events were observed in coincidence with a correlated recoil proton leads to the conclusion that there are very few pp pairs in the nucleus and the knocked out protons predominantly originated from np pairs. Fig. 6 shows the extracted ratio of np/pp SRC pairs in the measured nuclei. As can be seen, np-SRC pairs are observed to dominate over pp-SRC pairs even in neutron-rich, heavy nuclei.

The observed np-SRC dominance in heavy nuclei is a non-trivial result since, in these heavy nuclei, proton-proton pairs from different shells can create non l=0 pairs with non-zero spin that are also sensitive to the tensor part of the NN-interaction, thereby diminishing the observed np dominance observed in light nuclei. The observed np-SRC pair dominance also implies that in heavy, neutron-rich nuclei the high-momentum tail contains the same number of neutrons and protons, leaving the excess neutrons to occupy low-momentum states (see Fig. 7). This suggests that in neutron-rich nuclei there can be an inversion of momentum sharing between protons and neutrons where protons (i.e. the minority) have larger average momentum. This inversion is expected to be universal for any two-component Fermi systems with a short-range interaction between the different Fermions. This inversion and its universality have wide-ranging implications for calculations of the isospin dependence of the EMC effect in neutron-rich nuclei, the kinetic term of the nuclear symmetry energy at supra-nuclear densities, neutrino-nucleus scattering, and ultra-cold atomic gases.

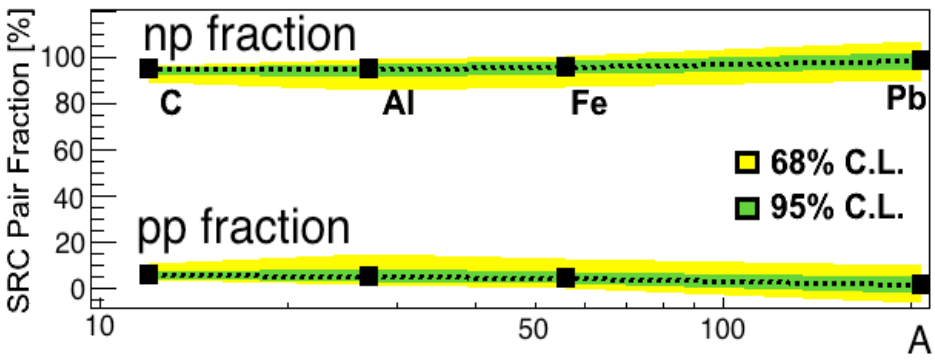

Fig 7: The extracted fractions of np (top) and pp (bottom) SRC pairs from the sum of pp and np pairs in nuclei in the missing-momentum range of 300–600 MeV/c. The inner and outer (green and yellow online) bands reflect 68% and 95% confidence levels, respectively.

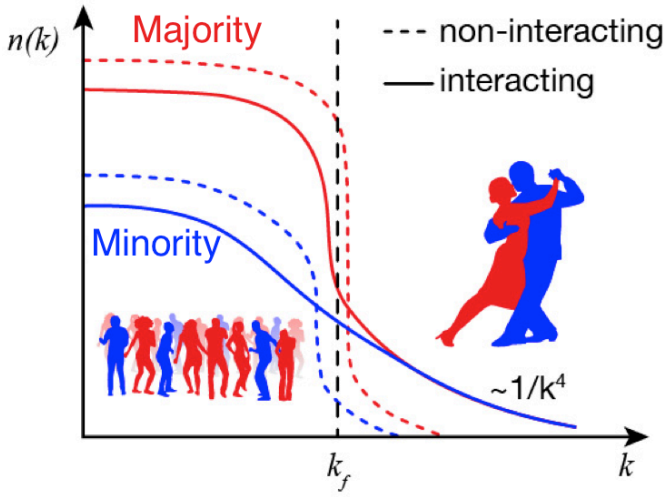

Fig 8: A schematic representation of the main characteristics of the momentum distribution, n(k), of asymmetric nuclei. This characteristic momentum distribution is expected to be universal for any two-component imbalanced Fermi system with a short-range interaction between different Fermions. The dashed lines show the standard non-interacting system while the solid lines show the effect of including a short-range interaction between different Fermions. Such interactions create a high-momentum ($k>k_F$) tail. This is analogous to a dance party with a majority of girls, where boy-girl interactions will make the average boy dance more than the average girl, and hence the boys will have a larger average momentum.

2.2. Impact of SRCs on other phenomena

Below, we list various aspects of nuclear, particle, astro- and atomic physics that are affected by our understanding of 2N-SRC pairs. The measurement proposed here will offer valuable insight to the structure and dynamics of 2N-SRC pairs in medium and heavy, symmetric and asymmetric nuclei, which will impact our understanding of these phenomena.

2.2.1. The EMC effect and the NuTeV anomaly

The deep inelastic scattering cross section for scattering from bound nucleons differs from that from free nucleons. This phenomenon, first discovered 30 years ago, is known as the EMC effect, and its origin is still not fully understood [29-32]. Recent experimental results [15,16], in addition to theoretical models, indicate a strong correlation between the size of the EMC effect and the number of SRC pairs in nuclei, indicating the possibility that both stem from high momentum (i.e., large virtuality) nucleons in the nucleus. A new 12 GeV Hall-C experiment was recently approved to measure semi-inclusive deep inelastic scattering (DIS) off of the deuteron by "tagging" the DIS scattering with high momentum recoiling protons or neutrons emitted at large angle relative to the momentum transfer [32]. The proposed measurement on the deuteron will have important implications for explaining the EMC effect and its relationship to SRCs.

Theoretical calculations show that an isospin-dependent EMC effect in neutron-rich nuclei, and in particular iron, could explain the NuTeV anomaly. The latter is a three standard deviation difference from the Standard Model prediction in the measurement of the electroweak-mixing (Weinberg) angle using neutrino scattering from iron [33]. While original analysis employed a mean-field model to explain the possible existence of such an isospin dependence, recent calculations show that, if the EMC effect is indeed related to high-momentum nucleons in nuclei, an observed dominated of np-SRC pairs in heavy nuclei can also lead to an isospin-dependent EMC effect, which can, in turn, supply an alternative, quantitative explanation of the NuTeV anomaly.

2.2.2. Neutrino-nucleus scattering

Traditional analyses of neutrino-scattering experiments use a non-interacting, relativistic Fermi gas model to describe the nucleus. Recent, high-precision measurements of neutrino and anti-neutrino scattering off of carbon nuclei, made by the Minerva collaboration, show the limitation of this approximate description and the need to include the effects of np-SRC pairs both in models of the scattering reaction and the detector response [21,22].

A recent conference at the Institute for Nuclear Theory (INT) [] focused on the current understanding of the charged-current, quasi-elastic neutrino-nucleus scattering process and its effect on the extraction of neutrino oscillation parameters, the neutrino mass hierarchy, and standard-model CP violation. It was shown that in order to achieve the required precision levels needed to facilitate next generation oscillation experiments, an improved understanding of neutrino-nucleus interaction is needed, and, in particular, a better description of the effect of correlations is required.

Electron- and proton-scattering measurements can provide vital input to such analyses, and, as many of the next-generation experiments are expected to use heavier nuclei as targets (e.g. Argon nuclei), additional high-precision information on correlations in such nuclei and their effect on both the high-momentum tail of the nuclear spectral function and many-body final states is required.

2.2.3. Cold nuclear matter and nuclear symmetry energy

2.2.3.1. The nuclear Symmetry Energy

The nuclear symmetry energy describes how the energy per nucleon in nuclear matter changes as a function of the proton fraction. Knowledge of the density dependence of the nuclear symmetry energy, and, in particular, its value at supra-nuclear densities, is important for various aspects of nuclear-astrophysics [34]. It determines the neutronization of matter in core-collapse supernovae, the properties of nuclei involved in r-process nucleo-synthesis, and the cooling rate and equation-of-state of neutron stars. The latter directly affects our knowledge of various properties of neutron stars, including their crust thickness and mass-radius relation. See Ref. [34] for a recent review.

While the value of the symmetry energy at nuclear saturation density is relatively well constrained by terrestrial measurements and astrophysical observations [34], its value at supra-nuclear densities and its general density dependence is not. This is largely due to uncertainties in the tensor component of the nucleon-nucleon interaction. Recent calculations show that the inclusion of high-momentum tails, dominated by tensor-force-induced np-SRC pairs, dramatically soften the nuclear symmetry energy at supra-nuclear densities [20] (See Fig. 9 for one such calculation).

The measurement proposed here will study in detail the dominance and absolute amount of np-SRC pairing in heavy asymmetric nuclei and, in particular, its dynamics as a function of the nuclear asymmetry. These measurements will help validate and constrain modern calculations.

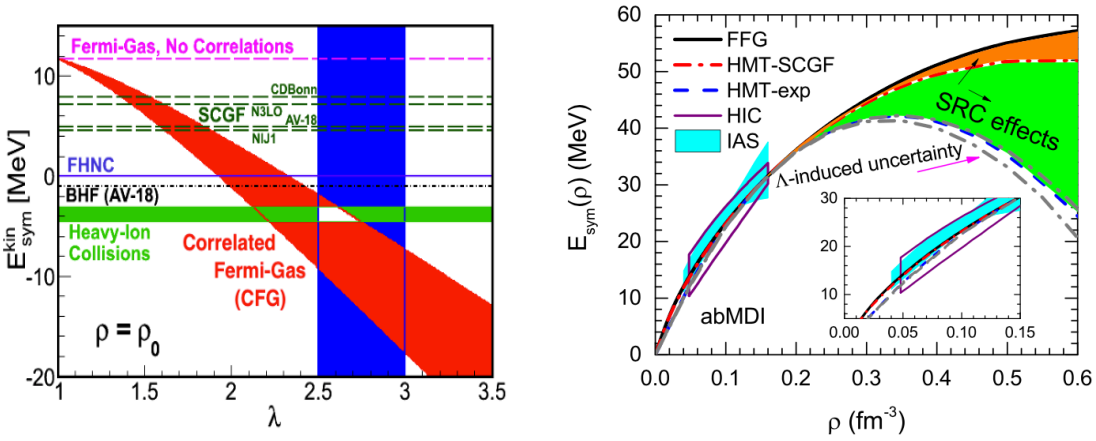

Fig 9: Left: Calculation of the kinetic part of the nuclear symmetry energy (difference between the kinetic energy on nucleons in pure neutron matter and symmetric nuclear matter) using various theoretical models, the simple Fermi-Gas model and the Correlated Fermi-Gas (CFG) model which accounts for np-SRCs. The CFG model calculation is shown as a function of the SRC cutoff parameter. See Ref. [] for details. Right: possible impact of SRCs on the nuclear symmetry energy at high densities (taken from a review paper by B.A. Li et al., to appear in Progress in Particle and Nuclear Physics).

2.2.3.2. Cooling rate of neutron stars

Theoretical analysis of neutrino cooling data indicates that neutron stars contain about 5 to 10% protons and electrons in the crust. Calculations show that np-dominance of SRC pairs in asymmetric nuclei and nuclear matter can cause the protons to heat up, bringing a large fraction of them above the proton Fermi momentum, opening holes below the Fermi momentum. The existence of such fast protons and the resulting holes in the Fermi sphere could allow for some direct, rather than modified, Urca cooling of neutron stars, even below threshold [19]. Since direct Urca cooling is about 10^6 times faster than modified Urca cooling, small changes could have a disproportionate impact on the cooling rate and the star lifetime.

New, high-precision data on the dynamics of 2N-SRC pairs in heavy nuclei and their dependence on the nuclear asymmetry will improve the accuracy and increase the reliability of such calculations.

3. Goals and significance of the proposed experiment

Exclusive, high-momentum, high-energy transfer (hard) reactions are ideal tools to study SRCs. The advantages of hard proton-induced reactions compared to those induced by leptons stem from:

1. The strong s-dependence of these processes which results in a very strong preference for scattering off of forward-going, high initial momentum nucleons,
2. Large momentum transfer that can be achieved at large angle scattering,
3. Large cross sections, which allow (in exclusive measurements) for better statistics and better signal/random coincidence background ratios.

We list below some specific objectives that can be achieved.

3.1. SRC Isospin Structure and the Tensor Force

The unique signature of the tensor force dominance is the large ratio of np to pp SRC pairs observed in measurements of symmetric nuclei (i.e. ^{4}He and ^{12}C). The measured ratios of np to pp SRC pairs deduced from the JLab and BNL data are shown in Fig. 5 and 6.

The BNL data include a small sample of struck protons and recoil neutron pairs only. We propose here new simultaneous exclusive triple coincidence measurements of all the struck/recoil proton/neutron combinations.

Aside from being the very first triple coincidence measurement of the A(p,2pp) reaction; this measurement, together with the A(p,2pn) measurement, will allow the study of the isospin ratio of SRC pairs as a function of their relative momentum. Of particular interest is the study of the number of pairs in very asymmetric ($N \neq Z$) nuclei such as ^{107}Ag.

The 6 GeV JLab experiment measured 18 times more np than pp pairs at 400–600 MeV/c relative momentum and observed a crude decrease in the ratio when going up to 850 MeV/c. This decrease, which is currently under further study, may have been due to the scalar nature of the repulsive core of the NN-interaction. However, the large bin-size and the large statistical uncertainties of the measurement prevented detailed study of this decrease. Strict constraints on theoretical estimates for the transition of the NN-interaction from the tensor dominant region to the (scalar) repulsive core were not possible.

The proposed measurement of A(p,2pn)/A(p,3p) ratio as a function of the missing momentum, with high statistics, will allow us to map the pn/pp ratio as a function of the missing momentum over a broad range. We also propose to study the lower nucleon relative momentum where the np/pp ratio is also expected to be smaller than that measured at 300–600 MeV/c.

3.2. C.M. and Relative Momentum Distributions of SRC pairs

Fig. 11 shows the low statistics BNL data for the reconstructed SRC c.m. and relative momentum distributions in ^{12}C and the preliminary analysis of the width of the c.m. momentum distribution of 2N-SRC pairs in various nuclei. The electron scattering data shown include results from JLab Hall-A (^{4}He and ^{12}C) and *preliminary* results from Hall-B (^{12}C, ^{27}Al, ^{56}Fe, and ^{208}Pb). Also shown are various theoretical predictions detailed below. While it is clear that the c.m. momentum is small ($k_{c.m.} < k_F$), the low-statistics of these measurements and uncertainties in the large acceptance corrections of the BNL and Hall-A measurements, prevent us from performing detailed quantitative analysis of the data and making a meaningful comparison of the A-dependence with calculations. Studies of these distributions for different nuclei with higher statistics and good resolution are clearly needed.

The proposed measurement will allow us to study the shape of the c.m. distributions with high statistics (which have so far been assumed to be Gaussian), and will allow for a detailed quantitative comparison with theory. Comparing these distributions for pn and pp pairs is also a unique aspect of the proposed measurement, not previously possible. Fig. 12 shows theoretical predictions by the Ghent group for the C.M. momentum distribution of a $^{1}S_0$ pair, as well as the average for all pairs [9,37]. The $^{1}S_0$ pairs are expected to be the dominant SRC pairs in nuclei.

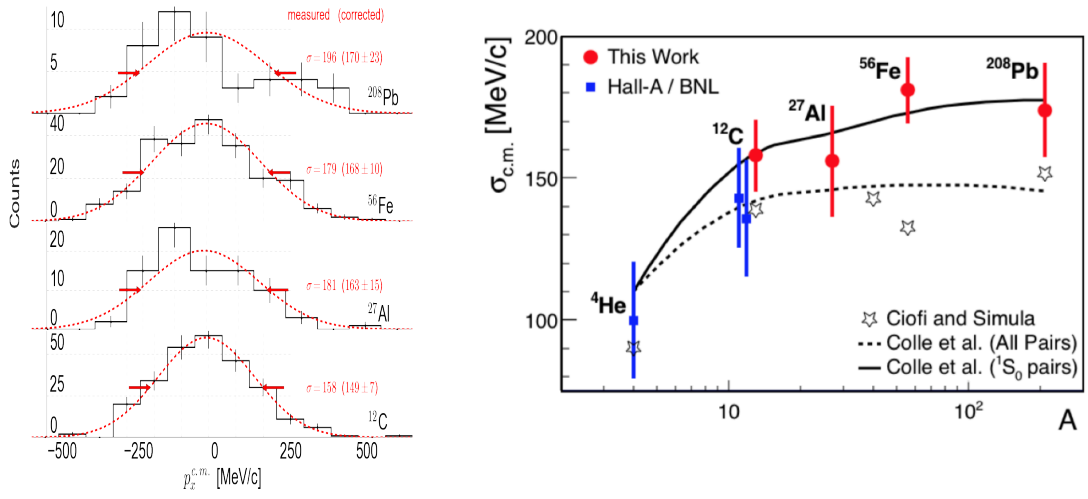

Fig. 12: Left: SRC pairs c.m momentum distributions as extracted from a recent measurement at JLab Hall-B. Right: extracted width of the c.m. momentum distribution for various nuclei from the BNL and JLab Hall-A data and the preliminary results from JLab Hall-B. The data are compared with various theoretical calculations.

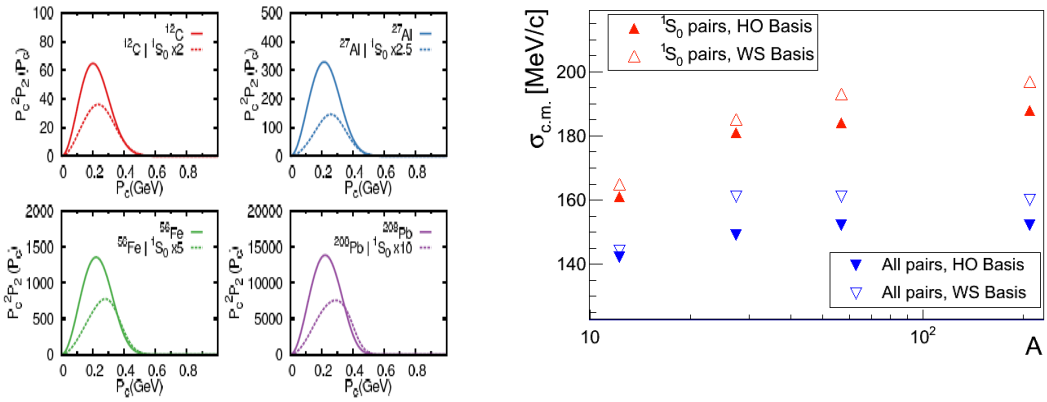

Fig. 13: Preliminary calculations by the Ghent group of the c.m. momentum distribution for $^1S_0$ pairs, as well as for the average for all pairs. The shell model calculations (left panel) were fitted to Gaussians and the widths are shown in the right pannel.

3.3. Mapping the Transition from Mean Field to SRC

Fig. 3 shows that an amazingly sharp transition between the mean field and the SRC domains, even with the poor statistics of the BNL data. Higher statistics data will tell us much more about this intriguing transition.

The proposed measurement will have the required statistics and resolution to study this process as a function of the missing mass of the struck proton in an SRC np-pair. Note also that for momenta close to the Fermi sea level, the relative contribution of pp SRCs could be significantly larger than for the kinematics studied at BNL.

3.4. Reaction Mechanism

The anticipated high-statistics experiment should allow detailed tests of the reaction mechanisms to be carried out. This would involve testing that the decay of the SRC does not change with the squared momentum transfer (t) to the struck nucleon. Comparing the BNL and JLab data, obtained at –t values close to 2 and 5 GeV^2, indicates that factorization holds in this range. Determining the minimal values for -t for which factorization still holds would be important for understanding the dynamics of the reaction. This would also allow for a practical application: to plan studies of the structure of unstable nuclei in A(p,2p) reactions with relativistic beams of unstable nuclei. Checking the factorization of the cross section as a product of the elementary cross section times a decay function is critical for determining how low in t and u one can measure, and thus the SRC event rate. Note that for exploring nucleons with momentum of 400 MeV/c and less, the requirement of large momentum transfer to the struck nucleon is somewhat less important than for the study of the higher missing momentum range as was done at JLab.

Studying the low t limit of the validity of SRC studies might allow performing future measurements in inverse kinematics using high-energy radioactive beams at FAIR.

4. Experiment

4.1. Kinematics

The typical kinematics for a triple coincidence event is shown in Fig 14. The incident proton momentum is P_{beam}, and the scattered proton and the forward knockout proton or neutron are P_1 and P_2 respectively. The recoil nucleon has momentum P_{recoil}. P_{miss} is the 3-momentum of the struck nucleon before the reaction. In the Plane Wave Impulse Approximation (PWIA) for a pair at rest, P_{miss} is equal in size and opposite to the 3-momentum of the recoil nucleon.

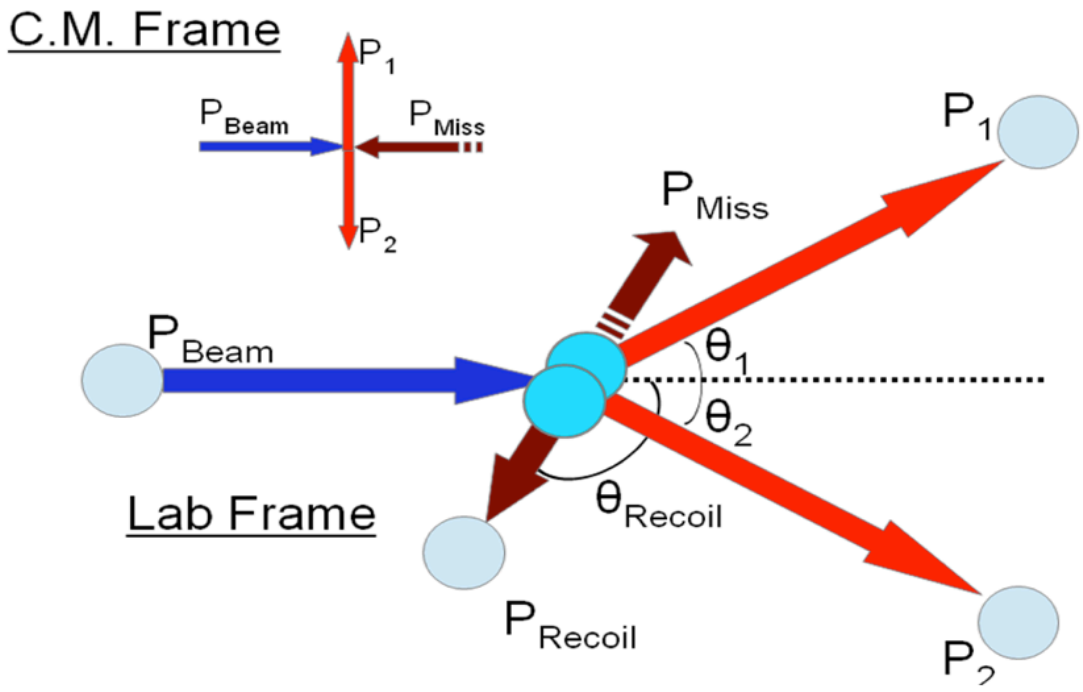

Fig. 14: The kinematics of the 90° c.m. scattering off a proton in a SRC pair.

For the simulation, we assumed a pair of nucleons with a symmetric 3D Gaussian c.m. momentum distribution (with a width of σ=140 MeV/c based on theoretical

predictions and previous measurements) and a relative momentum distribution proportional to k^{-4}, for $0.25 < k < 1$ GeV/c.

Fig. 15 shows the SRC simulation results for the A(p,2pN) reaction for a proton beam energy of 4.5 GeV (5.3 GeV/c momentum). The imposed kinematical constraints are:

1. Energy conservation.
2. Momentum conservation.
3. Scattering: $\theta_{cm} = 90^o \pm 30^o$
4. Co-planar events: $\Delta\Phi = 180^o \pm 20^o$
5. $|s| = (p_1 + p_2)^2 \geq 2\ (GeV/c)^2$
   $|t| = (p_{beam} - p_1)^2 \geq 2\ (GeV/c)^2$
   $|u| = (p_{beam} - p_2)^2 \geq 2\ (GeV/c)^2$

6. SRC dominance:
   $|P_{miss}| \geq 250 \frac{MeV}{c}$

The forward going protons mostly scatter at laboratory angles of 18°–45° relative to the beam with momentum from 1.0–5.0 GeV/c while the backward going recoil nucleon can be detected at laboratory polar angles of 100°–160°.

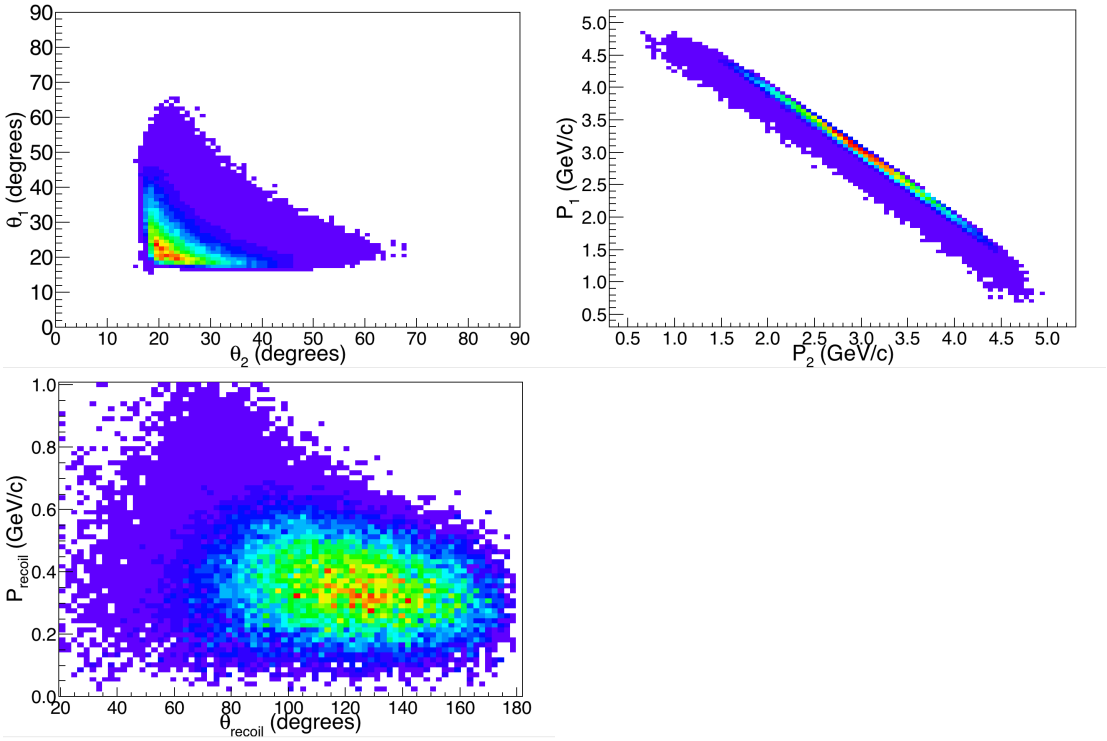

Fig. 15 (color online) Results of the simulations of 90^0 c.m. scattering off of protons belonging to SRC pairs for a 4.5 GeV (5.3 GeV/c momentum) proton beam, weighted by the s^{-10} scaling of the cross-section. The top plots show the correlation of the two polar angles (left top) and momenta (right top) of the forward going protons. The left bottom panel shows the correlation of the polar angles of the recoil nucleons with their momenta.

4.2. Experimental Setup

4.2.1. Detection System

For the unambiguous identification and detection of SRC reactions, one requires a detection system composed of two parts: a forward detector and a backward detector. The forward detector measures the two leading protons from a 90^o scattering in the c.m., mostly scattered at laboratory polar angles of 18^o–45^o relative to the beam and momenta ranging between 1.5-5 GeV/c. The forward detector also forms the event trigger. The backward detector measures the recoil nucleon emitted from the SRC pair breakup in coincidence with the forward going protons. We propose to use the HADES spectrometer as the forward detector and the dedicated large-acceptance REcoil Nucleon Detector (REND) as the backward detector.

Fig. 16 shows the schematic of the backward detector system. The detector consists of one large scintillator wall and two smaller side scintillator walls (green color). Part of the RICH detector of HADES and the relevant support structure (red color) can be seen at the front of the schematic while part of the last quadrupole magnet of the accelerator in the HADES cave (yellow) can be seen at the back of the schematic.

For the central plastic scintillator wall, we plan to use a part of the modular High-Resolution Neutron Time-of-Flight Spectrometer for R^3B (NeuLAND) [38]. The dimensions of the active volume of this part of NeuLAND are 250x250x60 cm^3, divided into 6 modules, 10 cm thick each. Each module consists of 2 crossed planes of plastic scintillator bars, each plane consisting of 50 square plastic scintillator bars with dimensions of 250x5x5 cm^3, coupled to PMTs on both ends. The central scintillator wall will be placed vertically 165 cm away from the target plane (closest proximity plane assuming the RICH remains in place) and 80 cm above the beam plane (YZ plane in Fig. 16). The center of the active area is $\sim$ 3.0 m away from the interaction point while the closest (furthest) distance is $\sim$ 2.0 m ($\sim$4.0 m) away. The detector will cover laboratory angles between 115^o–155^o. Fig. 17 shows a detailed mechanical drawing of one module of NeuLAND together with its support structure, which can hold all six modules that we plan to use for the proposed measurement.

The overall dimensions of the active volume of each of the two small plastic scintillator walls are 70x70x40 cm^3. Each small wall consists of 8 planes with dimensions of 70x70x5 cm^3 and each of the planes is made of bars with dimensions of 5x5x70 cm^3 coupled to 2″ PMTs on both ends. The two walls are positioned symmetrically with respect to XZ plane and they have an inclination of 45^o with respect to YZ plane and 25^o with XZ plane (see fig. 16). The center of the each small wall is $\sim$ 1.6 m away from the interaction point and will cover laboratory angles of 123^o–147^o.

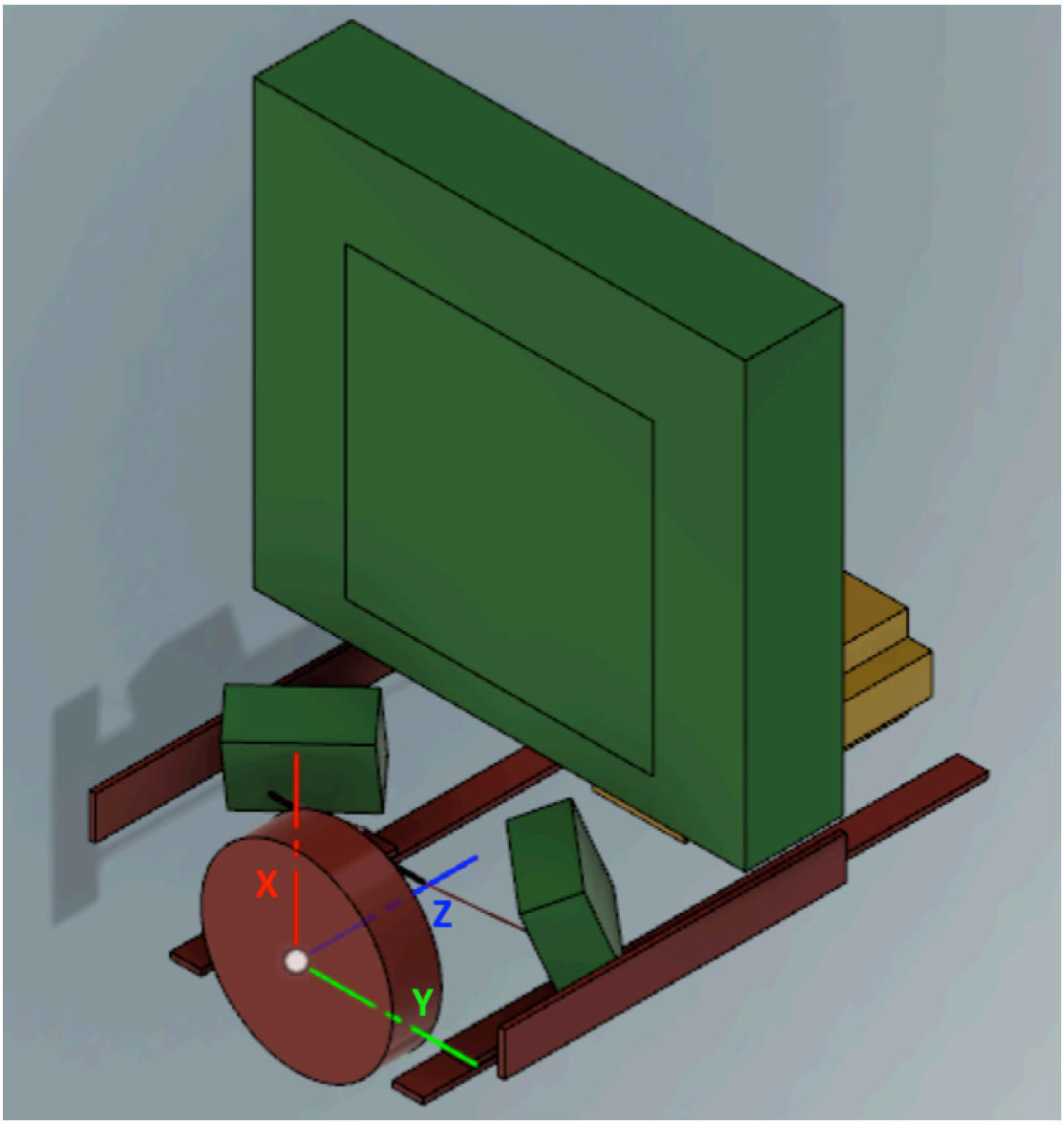

Fig. 16 (color online) Schematic sketch of REND detector placed at the back of HADES platform. The RICH detector and the relevant support structure are shown in red. A part of the last quadrupole magnet can be seen in yellow on the rear side of the platform. All volumes are drawn to scale.

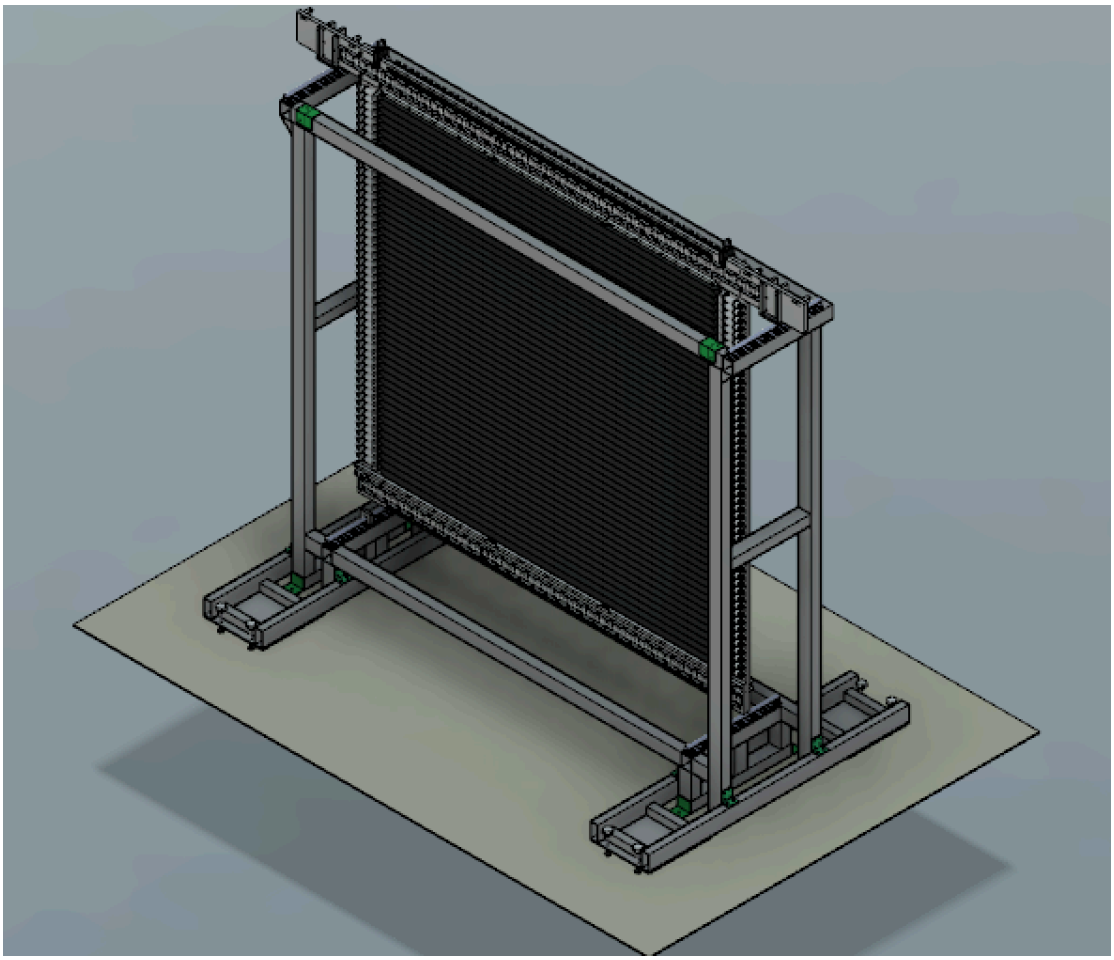

Fig. 17 The mechanical design of one module of the NeuLAND detector together with its support structure. The support structure can hold up to 6 double plane modules and can be used in the HADES cave as part of the REND detector.

4.2.2. Detector Resolution

The HADES start detector provides a t_0 reference time for the entire system. The forward tracking system of HADES is used to determine the forward proton momenta and scattering angles. The time-of-flight difference between the start detector and REND determines the speed of the recoil neutron given the distance of the interaction point to the scintillator. Based on the calculation of the speed of the nucleon, one can extract the momentum $P = \gamma mu$, the total energy, $E = m\gamma$, and the kinetic energy, $E_k = m(\gamma - 1)$. Assuming the time resolution of NeuLAND is δt =150 ps and that the uncertainty of the distance between the interaction point and the scintillator bar equals half its thickness δd =2.5 cm, the relative uncertainty on the nucleon speed is given by $\delta u/u = \sqrt{\left(\frac{\delta d}{d}\right)^2 + \left(\frac{\delta t}{t}\right)^2}$ given an average distance from the target to the front plane of NeuLAND d =3.0 m. The relative momentum uncertainty is given by $\delta P/P = \frac{1}{(1-\beta^2)}(\delta u/u)$ and the uncertainty on the total and kinetic energy are $\delta E/E =$

$\beta^2(\delta P/P)$ and $\delta E_k/E_k = \frac{\beta^2\gamma}{\gamma-1}(\delta P/P)$, respectively. Fig. 18 shows the absolute and relative uncertainty of momentum and the relative uncertainties of the kinetic and total energy as a function of the incident nucleon momentum.

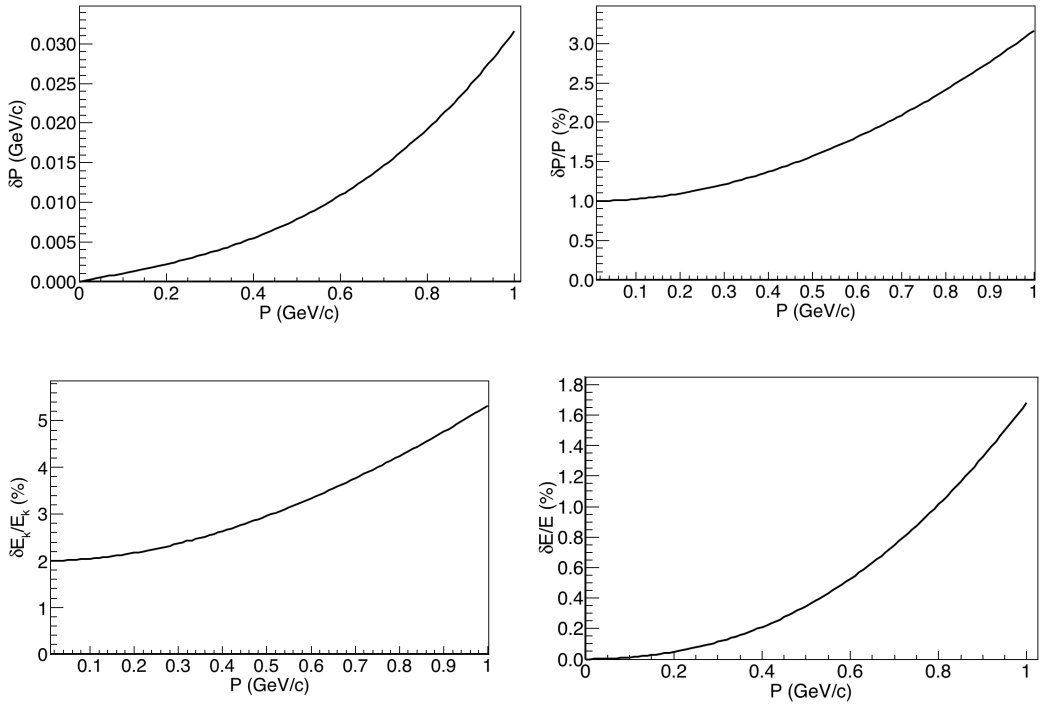

Fig. 18 A conservative estimation of the absolute (left top panel) and relative (right top panel) momentum uncertainties and the relative uncertainties on the total (left bottom panel) and kinetic (right bottom panel) energies as a function of the incident momentum of the recoil nucleon. The calculation assumes an average distance from the interaction point to the detector of 3.0 m and a time resolution of $\boldsymbol{\delta t}$ =150 ps.

4.2.3. Targets and Target Setup

For the first SRC measurement, we propose the use of the following targets: ^{12}C, ^{40}Ca and ^{107}Ag. For the future dedicated SRC measurement, we propose to use the following targets: ^{12}C, ^{40,48}Ca, ^{56}Fe and ^{107}Ag. Alternatively, we can use the targets: ^{12}C, ^{28}Si, ^{40}Ca, ^{107}Ag and ^{208}Pb. Other possible candidates are ^{112}Sn and ^{124}Sn. To obtain reasonable rates in fixed target, proton-beam measurements, targets densities of 2–5 gr/cm^2 (about 1%–3% interaction probability) are typically needed. To reduce random coincidence events in the analysis stage, and to allow low-energy protons to exit the target, one usually segments the target using up to 15 foils, spread over several cm.

In order to be sensitive to pp-SRC pairs, we need our foils to be thin enough so that recoiling protons can exit as well. In addition, the foils should be spread enough along the beam axis so that recoiling protons from one foil won't hit an adjacent foil. Considering the recoil nucleon angular distribution shown in Fig. 15, we propose focusing on recoiling nucleons in polar angles of 115^o – 155^o relative to the beam, which requires a foil separation of 5.5 mm for 2.0 mm wide

targets. Over a total distance of 5 cm we can place up to 10 such foils for each target.

For all of our planned targets, we propose having a total nuclear interaction probability of **2%**. The total thickness of each target (10 foils) that corresponds to 2% nuclear interaction probability can be seen in Table 1. The foil thickness, together with the thickness of the beam pipe (0.9 mm of carbon) and the path length of the protons in the air (minimum 1.6 m), determines the minimum recoil proton momentum that we are able to detect. The minimum recoil proton cut-off for all the targets is **200-210 MeV/c**. This minimum recoil proton cut-off will allow to us to observe the Migdal jump for pp-SRC pairs.

Targets	Target Thickness (g/cm^2)
^{12}C	1.7
^{28}Si	2.2
^{40}Ca	2.5
^{48}Ca	2.7
^{56}Fe	2.8
^{107}Ag	3.3
^{112}Sn	3.5
^{124}Sn	3.7
^{208}Pb	4.4

Table 1 List of targets and their thicknesses.

4.2.4. Trigger Scheme

For proton-beam running, we assume HADES can take data at a trigger rate of up to 20 kHz. The HADES trigger system can be configured in various ways.

For the first measurement of SRCs, which will run in parallel to di-lepton experiment using p+^{107}Ag reaction at an incident proton beam energy of 4.5 GeV, we propose the following plan which will allow to the di-lepton experiment to run mostly undisturbed using its own trigger scheme, while we acquire SRC data with a different trigger scheme.

To estimate the trigger rates for both trigger schemes, we used a simulation based on Ultra-relativistic Quantum Molecular Dynamics model (UrQMD) [39,40] transport code. The estimations presented below are based on an analysis of $5x10^5$ p+^{93}Nb simulated events. **The expected trigger rates for ^{93}Nb target will be very similar to the trigger rates expected from a ^{107}Ag target.** In the simulation, protons with kinetic energy of 4.5 GeV (5.3 GeV/c) impinge on a ^{93}Nb target. The statistics of this simulation is normalized to the expected number of interactions/s obtained with a maximum flux of $2x10^6$ p/s at a 4.5 GeV proton beam energy, impinging on a 2% interaction probability target. The trigger rates can be expressed with respect to hit multiplicity. Hit multiplicity is a variable that describes the number of charged particles that hit the detector.

Fig. 19 shows the trigger rates with respect to hit multiplicity for RPC detectors with progressively tighter trigger schemes for ^{93}Nb, assuming a flux of 2.0x10^{6} p/s. The trigger rate for multiplicity ≥ 1 is equal to ~**27 kHz**. The trigger rate for multiplicity ≥ 2 with at least two hits in opposite sectors (multiplicity ≥ 2 & opposite sectors) is equal to ~**7 kHz**. For the preferable trigger scheme for the SRC measurement (multiplicity ≥ 2 & opposite sectors & TOF ≤ 10 ns) the trigger rate according to this calculation is no more than ~**1.0 kHz**. Finally, the trigger rate for multiplicity exactly equal to 2 at opposite sectors having TOF ≤ 10 ns (multiplicity = 2 & opposite sectors & TOF ≤ 10 ns) is equal to ~**0.3 kHz**.

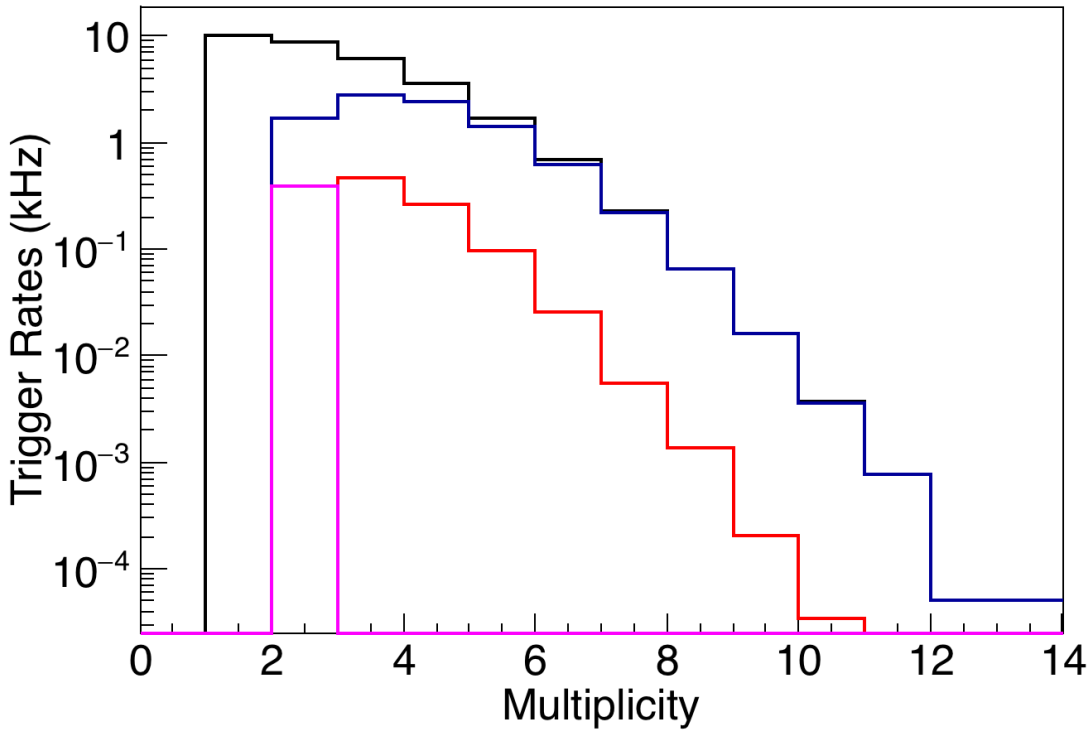

Fig. 19 (color online) Trigger rates as a function of multiplicity for ^{93}Nb target at 4.5 GeV incident proton beam energy assuming a flux 2.0x10^{6} p/s and 2% interaction probability. The **black line** shows the trigger rate with respect to hit multiplicity for multiplicity ≥ 1 (at least one charged particle at RPC detector). The **blue line** shows the trigger rate acquired with the condition that at least two opposite RPC sectors were hit by at least one charged particle (multiplicity ≥ 2 & opposite sectors). The **red line** shows the trigger rate acquired with the condition that at least two opposite RPC sectors were hit by at least one charged particle and the two leading charged particles had a time-of-flight less than 10 ns (multiplicity ≥ 2 & opposite sectors & TOF ≤ **10** ns). A 10 ns TOF corresponds to a proton with momentum of 1 GeV/c and a flight path of 2.2 m. Finally, the **magenta line** shows the trigger rate for the condition that only two opposite RPC sectors were hit by at least one charged particle and that the two leading charged particles had a time-of-flight less than 10 ns (multiplicity == 2 & opposite sectors & TOF ≤ **10** ns).

A more advanced estimation of the trigger rate was made with a GEANT3 simulation using as input the UrQMD events for p+^{93}Nb reaction at an incident proton kinetic energy of 4.5 GeV. Fig. 20 shows the trigger rates with respect to different trigger schemes assuming a flux of 2.0x10^{6} p/s and a 2% interaction

probability. The trigger rate for the RPC multiplicity ≥ 1 (N_{rpc}≥ 1) is equal to **~30 kHz (compared to ~27 kHz from UrQMD alone)**. The trigger rate, where the RPC multiplicity is greater or equal to 2 and at least two of the hits are at the opposite sector (N_{rpc}≥ 2 & opposite sector), is **~7 kHz (compared to 7 kHz from UrQMD alone)**. The trigger rate acquired under the condition that at least two opposite RPC sectors were hit by at least one charged particle and the two leading charged particles had a time-of-flight less than 10 ns (N_{rpc}≥ 2 & opposite sectors & TOF ≤ 10 ns) is equal to ~**3 kHz (compared to ~1.0 from UrQMD alone)** whereas the trigger rate for RPC multiplicity exactly equal to 2 (N_{rpc}= 2 & opposite sectors & TOF ≤ 10 ns) is **~1 kHz (compared to ~0.3 kHz from UrQMD alone)**. These estimations are comparable to the estimations that were acquired using the UrQMD transport code alone (without going through GEANT3) (see figure 19) and gives additional confidence as to the order of magnitude and the margin of error of these calculations.

We estimate that the trigger rate for the condition $N_{tof+rpc}$ ≥ 2 (at least two charged particle at HADES detector), which is the preferable condition for the di-lepton experiment, is equal to **~32 kHz**. Since the HADES DAQ will only be able to handle 20 kHz, the trigger rate has to be reduced by a factor of **1.6**. This can be achieved by either reducing the beam flux by **x1.6** or by pre-scaling the di-lepton DAQ system by the same factor. The latter will not hurt the statistics of the di-lepton experiment and will allow us to collect enough statistics for the SRC measurement.

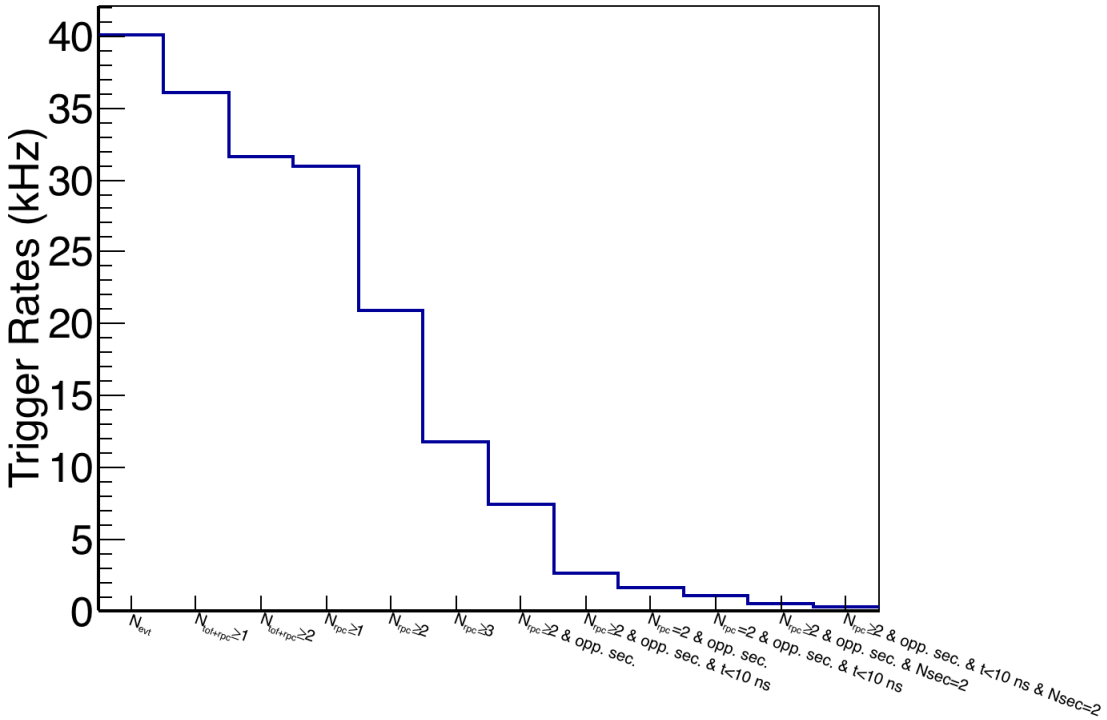

Fig. 20 Trigger rates as a function of different trigger schemes based on GEANT3 simulation using as input UrQMD events for the reaction p+^{93}Nb with a 4.5 GeV incident proton beam energy assuming a flux of 2.0x10^{6} p/s and 2% interaction probability.

For the future dedicated SRC experiment, we consider a trigger scheme that is based on information from the 6 HADES RPC sectors (covering polar angles of 18°–45°) and is optimized for SRC studies, focusing on detection of pp scattering at 90° in the c.m. frame. The characteristic topology for such scattering is two forward going protons with in-plane scattering angles of 18°–30°, momenta of ~2–5 GeV/c and opposite out-of-plane angles (see Fig. 15). In this topology, the RPC detector alone is sufficient for the selection of the two forward going protons in desired SRC events.

To estimate the trigger rates, we used a simulation based on the UrQMD transport code. The estimations presented below are based on analysis of 5×10^6 p+^{12}C, 8×10^6 p+^{56}Fe and 10^7 p+^{93}Nb interactions. In the simulation, protons with kinetic energy of 4.5 GeV (5.3 GeV/c momentum) are impinged on a Carbon/Iron/Niobium target. The simulation rate is normalized to the expected amount of interactions/s obtained with a 1×10^7 p/s, 4.5 GeV, proton beam impinging on a 2% interaction probability target.

Figs. 21, 22 and 23 present the trigger rates with respect to hit multiplicity with progressively tighter trigger schemes for three different targets namely ^{12}C, ^{56}Fe and ^{93}Nb. We found that a trigger scheme that requires at least two opposite RPC sectors hit by at least one charged particle and that the two leading charged particles had a time-of-flight less than 10 ns (multiplicity ≥ 2 & opposite sectors & TOF ≤ **10** ns) is ideal for the measurement of SRC pairs, being not too restrictive and making sure that the trigger rates are comparable to the maximum 20 kHz rate that the future HADES acquisition system is expected to handle.

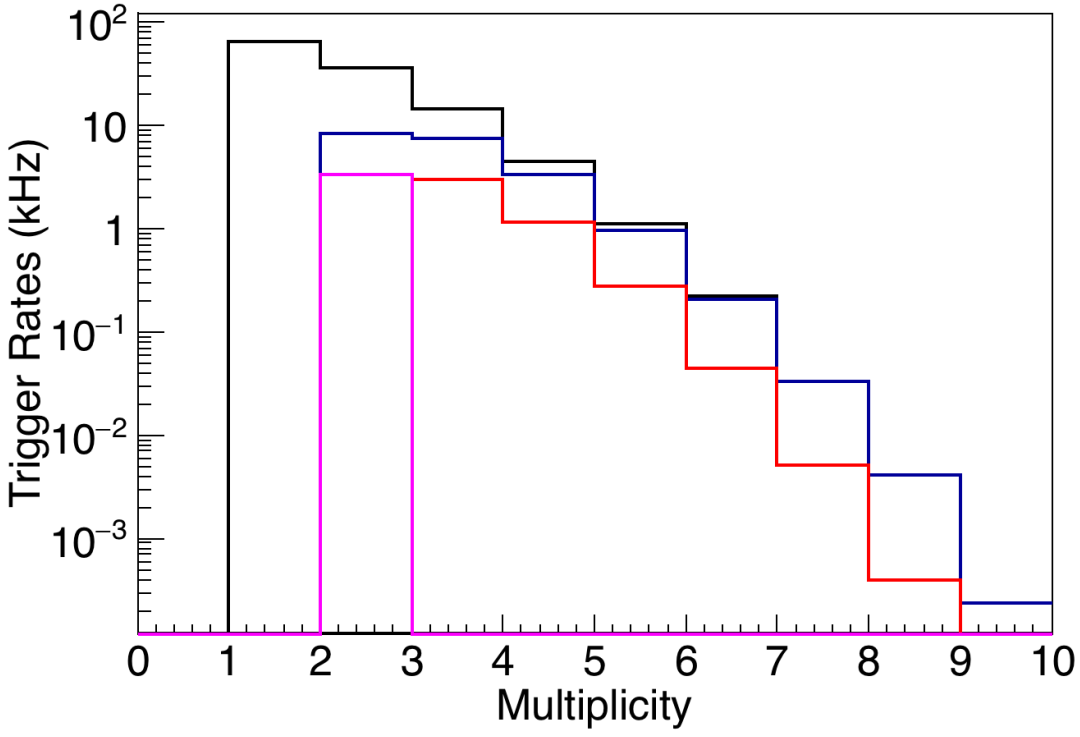

Fig. 21 (color online, lines as before) Trigger rates as a function of Multiplicity for ^{12}C target at 4.5 GeV incident proton beam energy, assuming a flux 1×10^7 p/s and 2% interaction probability.

Table 2 summarizes the resulting trigger rates for the ideal trigger scheme for the observation of the SRC events. The trigger scheme requires Multiplicity ≥ 2 at opposite RPC sectors of HADES and TOF ≤ 10 ns.

Target	Trigger rate (kHz)
^{12}C	8
^{56}Fe	7
^{93}Nb	6

Table 2: Simulated trigger rates for different targets, assuming a 4.5 GeV proton beam with flux of $1x10^7$ p/s and a 2% interaction probability target.

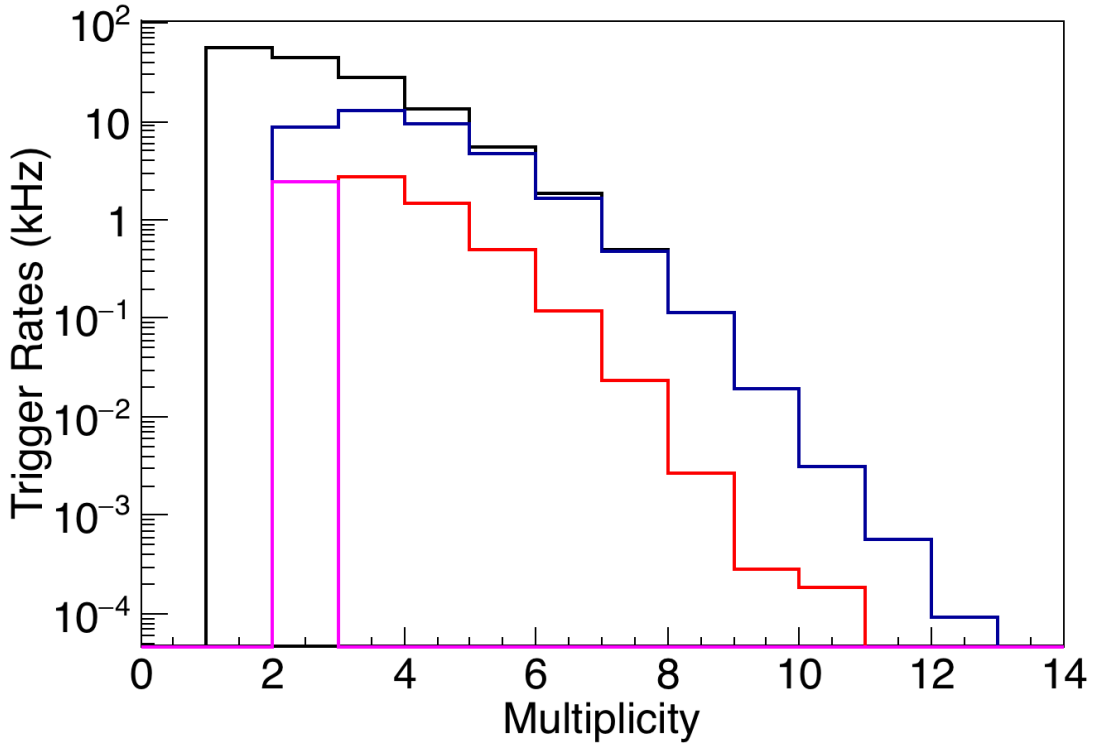

Fig. 22 (color online) Same as Fig. 21 for ^{56}Fe.

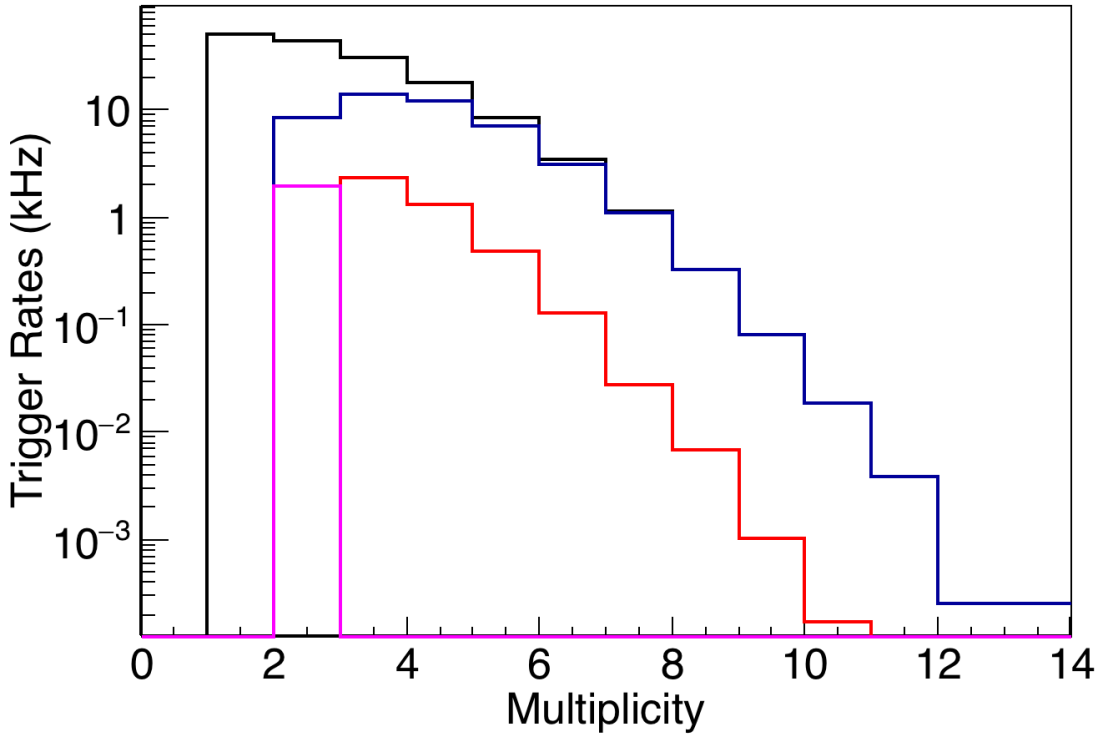

Fig. 23 (color online) Same as fig. 21 for ^{93}Nb.

As before, a more detailed estimation of the trigger rate was made with a GEANT3 simulation using as input the UrQMD events for p+^{93}Nb reaction at the incident proton kinetic energy of 4.5 GeV. Fig. 24 shows the trigger rates with respect to different trigger schemes assuming a flux of 1x10^{7} p/s and a 2% interaction probability. The trigger rate for the RPC multiplicity ≥ 1 (N_{rpc}≥ 1) is equal to **~156 kHz (compared to ~156 kHz from UrQMD alone)**. The trigger rate, where the RPC multiplicity is greater or equal to 2 and at least two of the hits are at the opposite sector (N_{rpc}≥ 2 & opposite sector), is **~40 kHz (compared to 47 from UrQMD alone)**. The trigger rate acquired under the condition that at least two opposite RPC sectors were hit by at least one charged particle and the two leading charged particles had a time-of-flight less than 10 ns (N_{rpc}≥ 2 & opposite sectors & TOF ≤ 10 ns) is equal to ~**12.5 kHz (compared to ~6 kHz from UrQMD)** whereas the trigger rate for RPC multiplicity exactly equal to 2 (N_{rpc}= 2 & opposite sectors & TOF ≤ 10 ns) is **~5 kHz (compared to 2 kHz from UrQMD)**. The rate of the preferred trigger is 12.5 kHz and well below 20 kHz trigger rate that HADES detector can handle.

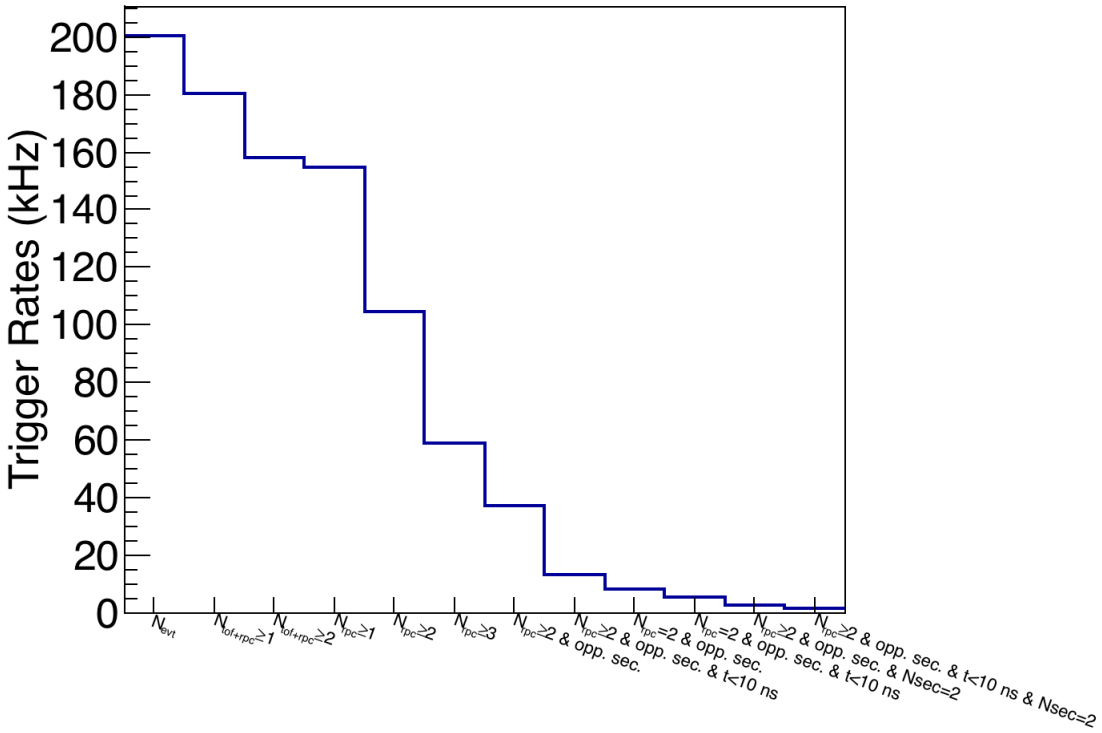

Fig. 24 Trigger rates as a function of different trigger schemes based on GEANT3 simulation using as input UrQMD events for the reaction p+^{93}Nb at 4.5 GeV incident proton beam energy assuming a flux of 1.0x10^{7} p/s and 2% interaction probability.

4.3. Rate estimations

4.3.1. A(p,2pn) and A(p,2pp) rates

A calculation of the triple coincidence rates for A(p,2pn) and A(p,2pp) was made using realistic angular and momentum resolutions of the HADES detector. These realistic resolutions were extracted from the official GEANT3 simulation of the HADES collaboration by shooting a 4.5 GeV proton beam on a ^{93}Nb target. The extracted resolutions were implemented in the kinematics simulation for SRC pairs presented in chapter 4.1.

Fig. 25 shows the polar angular resolution $\Delta\theta$, the azimuthal angle resolution $\Delta\phi$, the relative momentum resolution $\Delta P/P$, and the vertex resolution $\Delta Z * sin(\theta)$ with respect to polar angle θ, azimuthal angle ϕ and incident momentum of proton $|P|$. The dependence of $\Delta\theta$ on θ was observed to be mostly flat, with a value of ~0.06°, while a linear dependence was found between $\Delta\theta$ and $|P|$: $\Delta\theta = -0.016\text{xP} + 0.12$. No dependence of $\Delta\phi$ on θ, ϕ and $|P|$ was observed and an average value of $\Delta\phi = 0.28^{o}$ was used. A non-trivial relation was observed between the $\Delta P/P$, θ and $|P|$. Fig. 26 shows the correlation of $\Delta P/P$ as a function of θ and $|P|$.

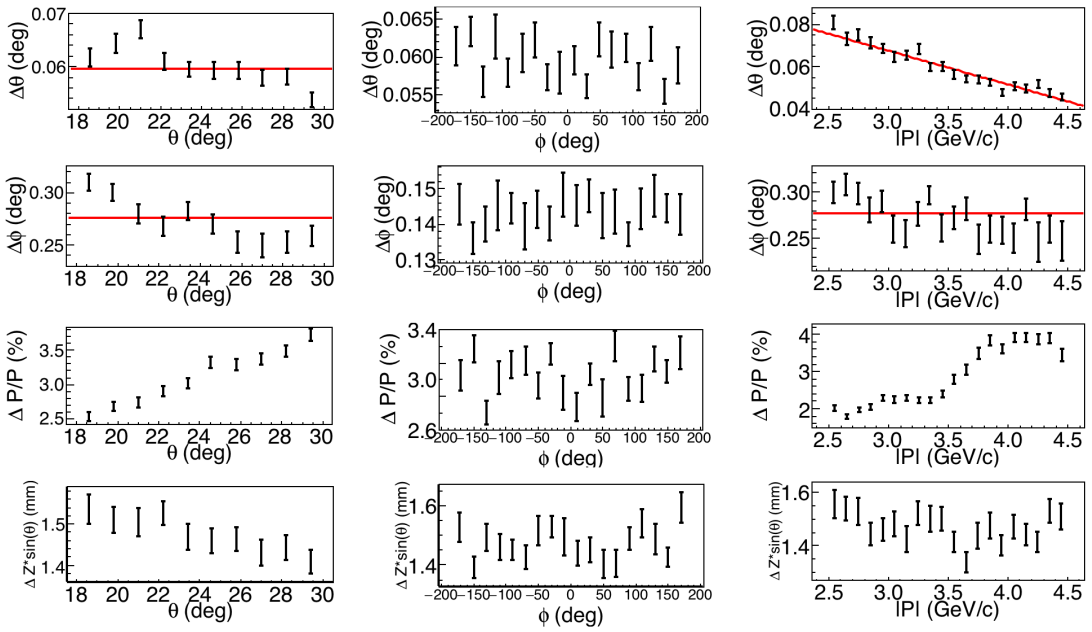

Fig. 25 The polar angle resolution $\boldsymbol{\Delta\theta}$ (1st row), the azimuthal angle resolution $\boldsymbol{\Delta\phi}$ (2nd row), the relative momentum resolution $\boldsymbol{\Delta P/P}$ (3rd row), and the vertex resolution $\boldsymbol{\Delta Z * sin(\theta)}$ (4th row) with respect to polar angle $\boldsymbol{\theta}$ (1st column), azimuthal angle $\boldsymbol{\phi}$ (2nd column) and incident momentum of proton $|P|$ (3rd column).

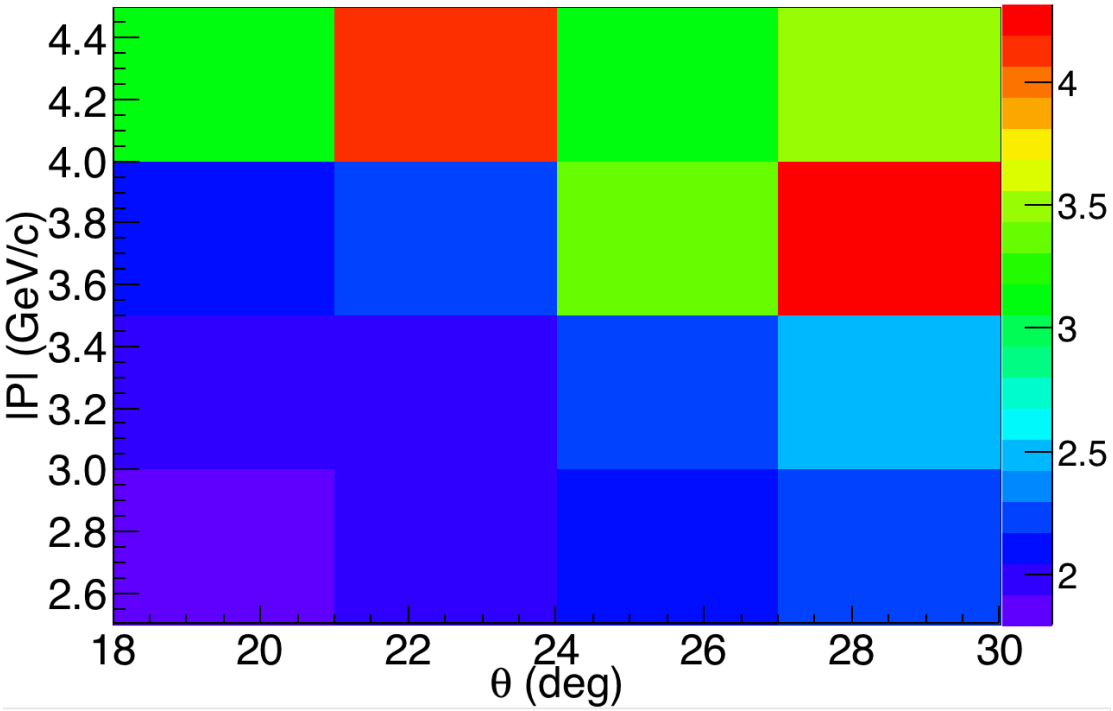

Fig. 26 (color online) The correlation map between $\boldsymbol{\Delta P/P}$ as a function of $\boldsymbol{\theta}$ and $|P|$. The color code shows the magnitude of $\boldsymbol{\Delta P/P}$(%).

Given HADES resolutions, we proceeded to the reconstruction of several characteristic kinematic variables for SRC events. An important variable among those is the P_{miss}, which is the 3-momentum of the struck nucleon before the reaction. Based on the conservation of momentum, P_{miss} can be reconstructed as the sum of momenta P_1 and P_2 minus the beam momentum P_{beam}, $P_{miss}= P_1 + P_2 - P_{beam}$. Fig. 27 shows the actual P_{miss} distribution and the reconstructed P_{miss} given HADES resolutions.

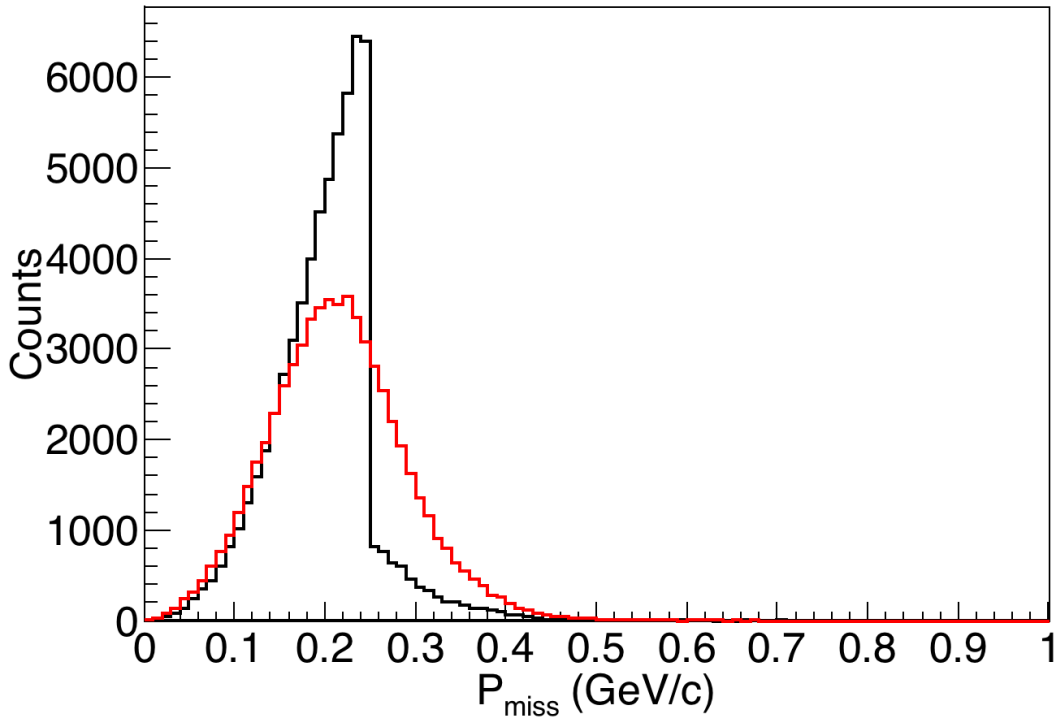

Fig. 27 (color online) Comparison of actual P_{miss} (**black curve**, assuming that 80% of the nucleons are in the mean field region and 20% lay under the SRC tail) with the reconstructed P_{miss} (**red curve**) based on HADES resolutions.

It is clear that there is a smearing of the initial distribution due to the resolutions of the $P_{1,2}$ momenta. This smearing leads to the need to identify the event region in the reconstructed P_{miss} spectrum originating from SRC tail with original $P_{miss} \geq 0.25$ GeV/c.

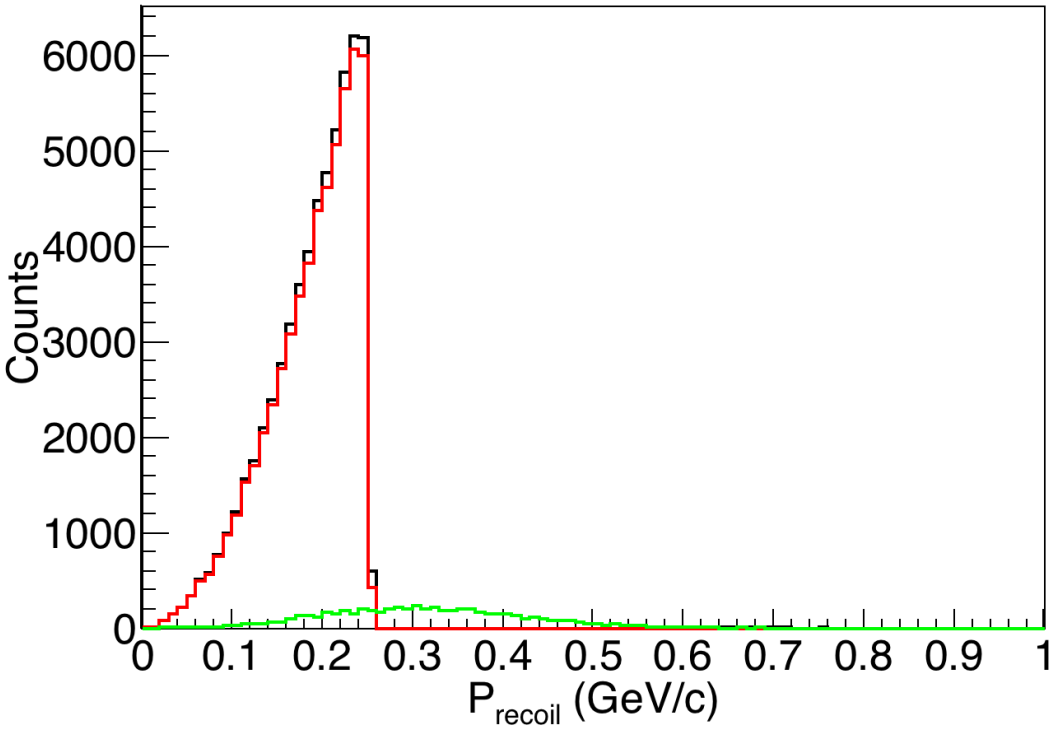

Fig. 28 (color online) The reconstructed P_{recoil} distribution (**black curve**) shown in **red are** the reconstructed P_{recoil} with original $P_{miss} \leq 0.25$ GeV/c. $P_{miss} \geq 0.25$ GeV/c are shown in **green**. A cut at $P_{recoil} \geq 0.27$ GeV/c will ensure the selection of events coming mainly from the SRC tail.

Requiring the additional detection of the recoil nucleon allows placing a lower cut on the reconstructed P_{miss}. Figure 28 shows the reconstructed P_{recoil} distribution and its decomposition to events with original P_{miss} above and below 0.25 GeV/c. A cut at $P_{recoil} \geq 0.27$ GeV/c effectively selects of recoil nucleons from the SRC tail. Given the cut on the reconstructed momentum of the recoil nucleon, we could reevaluate the cut on the reconstructed P_{miss}. We found that the P_{miss} cut can be as low as $P_{miss} > 0.25$ (see fig. 29).

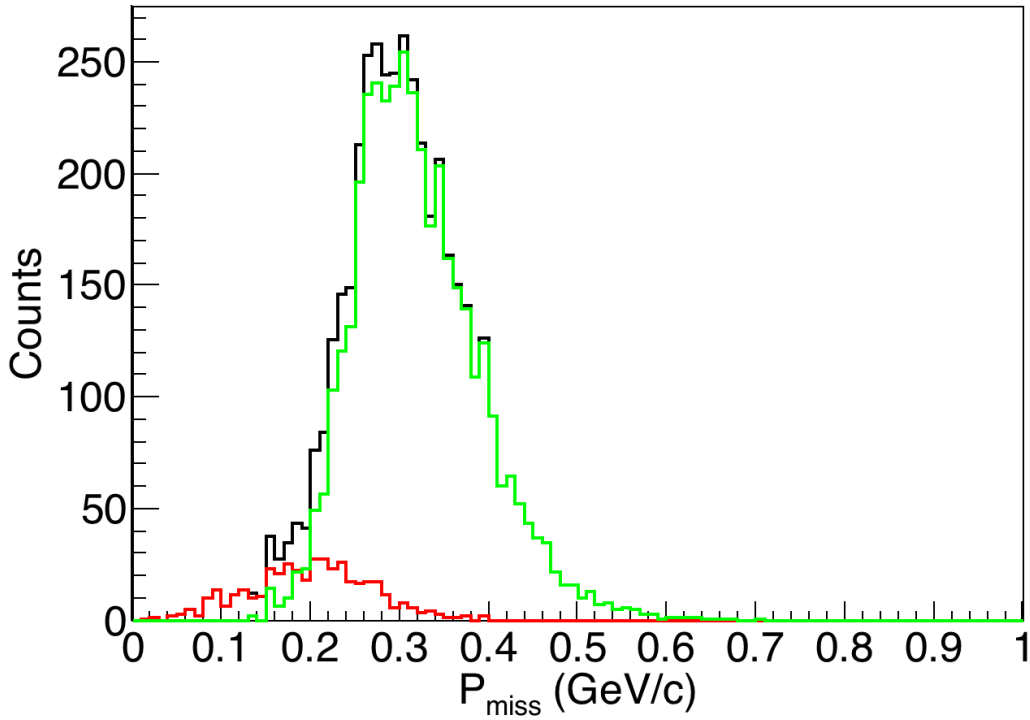

Fig. 29 (color online) The reconstructed P_{miss} distribution (**black curve**) together with the reconstructed P_{miss} with original $P_{miss} \leq 0.25$ GeV/c (**red curve**) and $P_{miss} \geq 0.25$ GeV/c (**green curve**). Given current resolutions, a cut at reconstructed $P_{miss} \geq 0.27$ GeV/c will ensure the selection of events coming mainly from the SRC tail.

One of the objectives of the proposed measurements is the observation for the first time of the Migdal jump (see chapter 2.1.2). Using the actual resolutions of HADES detector, we observed that the reconstruction of the opening angle cos ($\theta_{Pmiss,Precoil}$) between the recoil nucleon momentum and the initial momentum (P_{miss}) of the struck proton is unaffected as can be seen in Fig. 30.

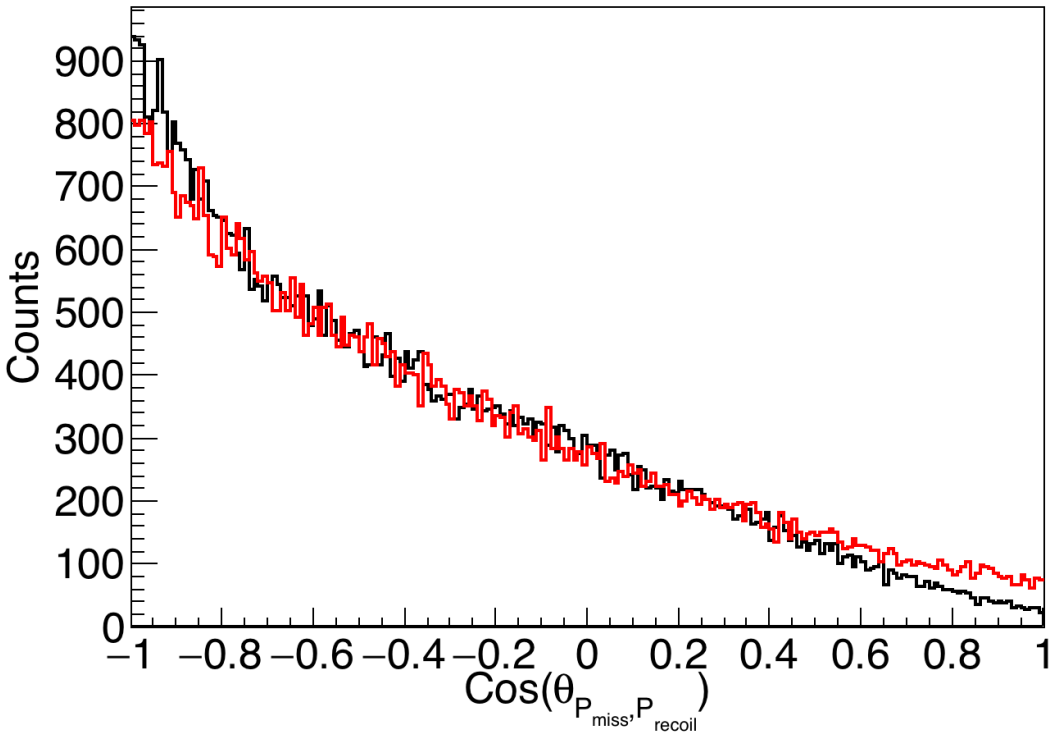

Fig. 30 (color online) The opening angle opening angle **cos** ($\boldsymbol{\theta_{Pmiss,Precoil}}$) between the recoil nucleon momentum and the initial momentum (P_{miss}) of the struck proton before (**black curve**) and after (**red curve**) resolution smearing.

Fig. 31 shows the correlation of the opening angle cos ($\theta_{Pmiss,Precoil}$) with the momentum of the recoil nucleon, P_{recoil} as it can be measured given the resolution of HADES detector.

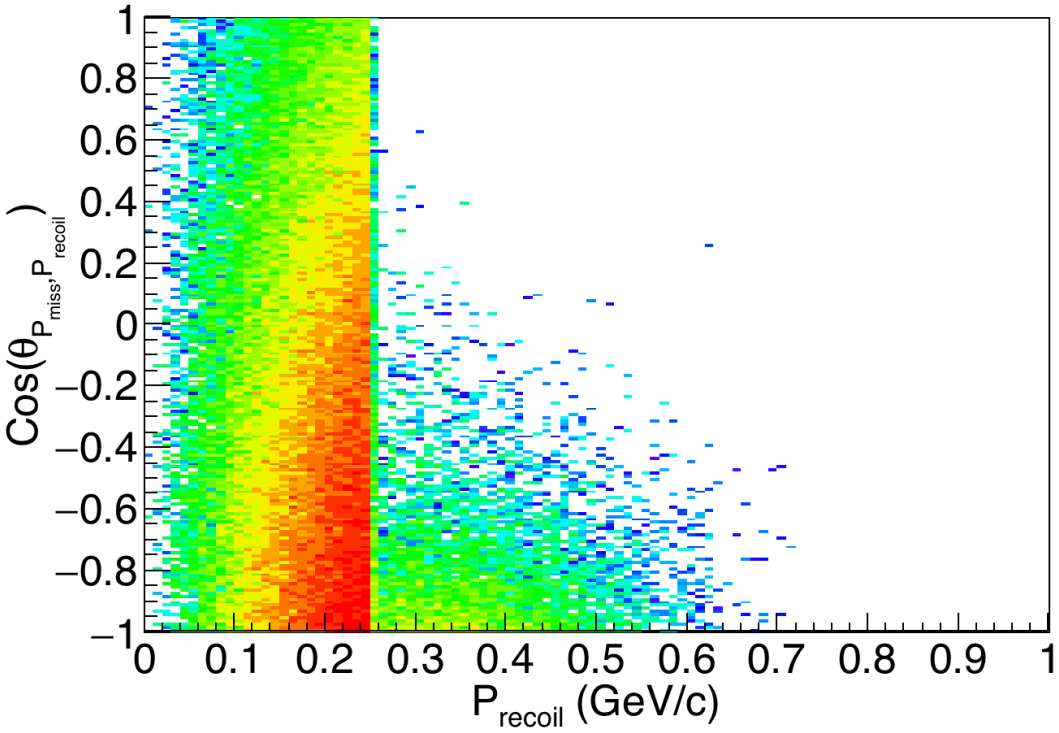

Fig. 31 The correlation between **cos** ($\boldsymbol{\theta_{Pmiss,Precoil}}$) and the momentum of the recoil nucleon.

Further comparisons between the initial and reconstructed variables were made for many other kinematic quantities. The comparisons indicate that, when using realistic HADES resolutions, SRC events can be identified and their properties can be quantified.

To validate the simulation code, we compared its outcome with the past-acquired data p+^{93}Nb at 3.5 GeV from HADES collaboration. The experimental parameters used in our analysis can be seen in Table 3.

Parameters	**Values**
Target Thickness	10^{24} protons/cm^2
Beam flux	2x10^6 p/s
Time	4.67 hrs
DAQ Efficiency	0.7
Downscaling Factor	3
Duty Cycle	83%
Target Transparency	0.2
Tracking Reconstruction	0.5

Table 3 Experimental parameters during the 2008 run of HADES collaboration on p+^{93}Nb at 3.5 GeV.

The data were initially skimmed to require exactly two protons in HADES acceptance. Fig. 32 shows the correlation of Mandelstam s with the sum of polar angles $\theta_1 + \theta_2$ for the two protons in the laboratory frame.

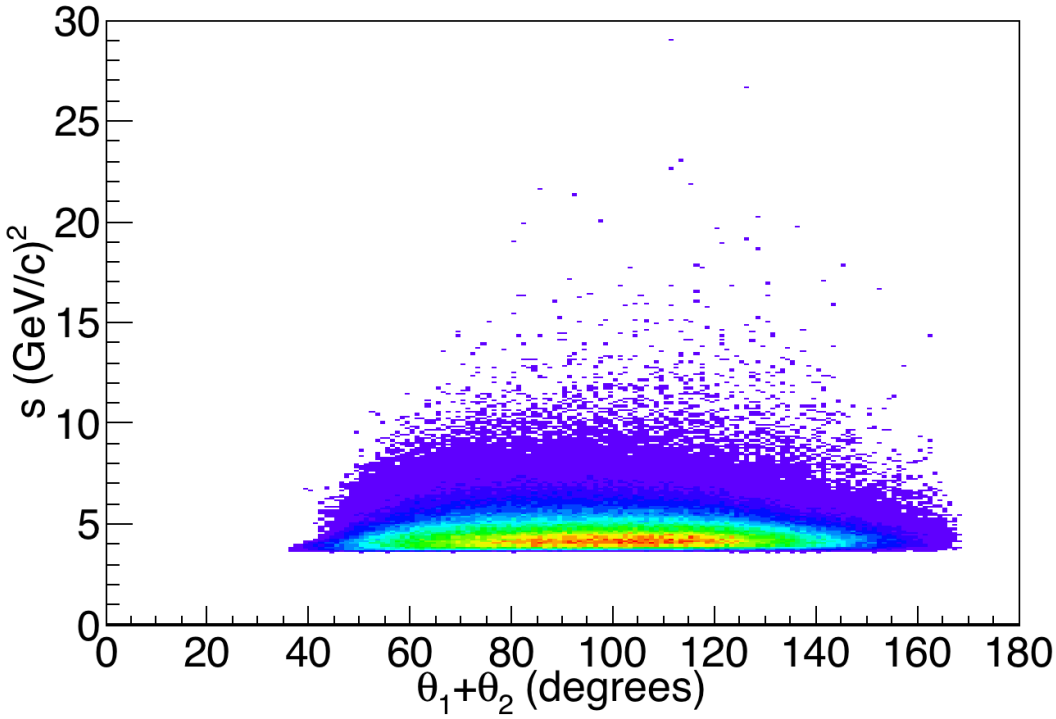

Fig. 32 The correlation of Mandelstam variable s with the sum of polar angles $\boldsymbol{\theta_1 + \theta_2}$ for the two protons.

Several analysis cuts were applied to the acquired data in order to identify the SRC event candidates. We picked co-planar events by requiring the difference of the azimuthal angles of the two protons to be $\Delta\phi_{lab} = 180° \pm 20°$. We required that the selected events have laboratory polar angles θ_{lab} from 18° to 85° and $\theta_{cm} = 90° \pm 30°$. We ensured the selection of hard scattering events by requiring all Mandelstam variables to be ≥ 2 (GeV/c)^2 and that these events come from the SRC tail by applying a P_{miss} cut: 0.5 (GeV/c) $\leq P_{miss} \leq$ 1.0 (GeV/c). Finally, we required the sum of the kinetic energies of the two outgoing protons to be $E_{1,k} + E_{2,k} \geq$ 3.2 GeV. A summary of all cuts can be seen in Table 4.

Quantities	Cuts
θ_{cm}	$60° \leq \theta_{cm} \leq 120°$
θ_{lab} of P_1,P_2	$18° \leq \theta_{lab} \leq 85°$
|s,t,u|	≥ 2 (GeV/c)^2
$\Delta\phi_{lab} = \lvert\phi_1 - \phi_2\rvert$ of P_1,P_2	$160° \leq \Delta\phi_{lab} \leq 200°$
P_{miss}	0.5 (GeV/c)$\leq P_{miss} \leq$1.0(GeV/c)
$E_{1,k} + E_{2,k}$	$\geq$3.2 GeV

Table 4 Analysis cuts for the identification of SRC events from the 2008 data acquired on p+^{93}Nb at 3.5 GeV.

Fig. 33 shows the correlation of Mandelstam s with the sum of polar angles $\theta_1 + \theta_2$ after cuts (left panel) in comparison to the SRC signature as predicted based on the simulation for the SRC kinematics. After applying the same cuts in the simulation and the data, a total of ≈75 events were observed in both cases. This adds additional confidence to the accuracy of the simulation.

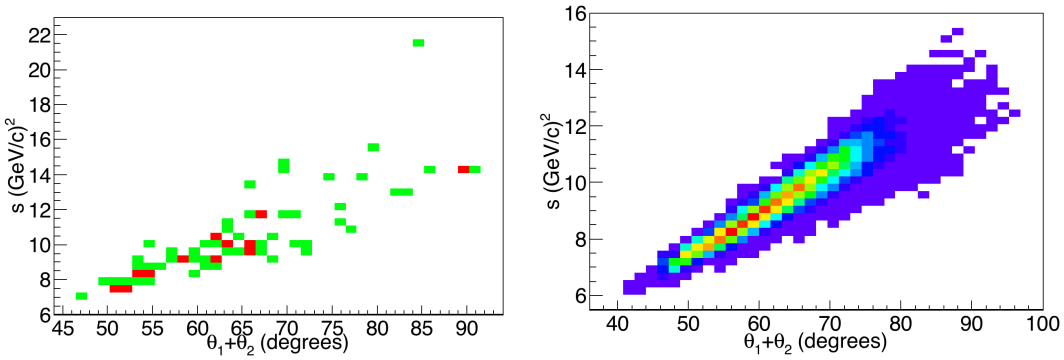

Fig. 33 The correlation of Mandelstam s with the sum of polar angles $\boldsymbol{\theta_1 + \theta_2}$ for the acquired data on p+^{93}Nb at 3.5 GeV after cuts (left panel) in comparison to the SRC events predicted by the simulation.

We assume that, in the targets we plan to use, 20% of the nucleons are in SRC pairs and that these pairs are 90% np, 5% pp, and 5% nn. The nuclear transparency for the two 2–5 GeV/c leading nucleons and the ~0.5 GeV/c recoil nucleon is ~ 20% [41]. The fraction of accepted recoil nucleons (due to the finite angular acceptance of the detectors) was found to be 30%. We assume a 3.3 g/cm^2 target (i.e. 10^{24} protons/cm^2) and an overall 50% recoil neutron detection efficiency given that we use a 60 cm thick part of NeuLAND and two 40 cm thick small plastic scintillator walls. Table 5 summarizes the assumptions made in the estimation of the amount of SRC events.

Parameters	Values
Target Thickness	10^{24} protons/cm^2
Beam flux for current run	2x10^6 p/s
Beam flux for future run	1x10^7 p/s
Time	28 days
Duty Cycle	10%
Target Transparency	0.2
Acceptance Factor	0.3
Tracking Reconstruction	0.5
Average neutron efficiency	50%

Table 5 A summary of the parameters assumed in the SRC simulation.

Apart from the aforementioned assumptions, the most-up-to date quasi-elastic pp experimental differential cross sections [42-45] were used as input into our SRC simulation together with the predictions from SAID model [46] which is valid below 3.7 GeV/c. Fig. 34 shows a summary of all pp quasi-elastic differential cross sections for $\theta_{cm} = 90^o$ data, for up to 14 GeV/C incident beam momentum in comparison to the SAID model predictions.

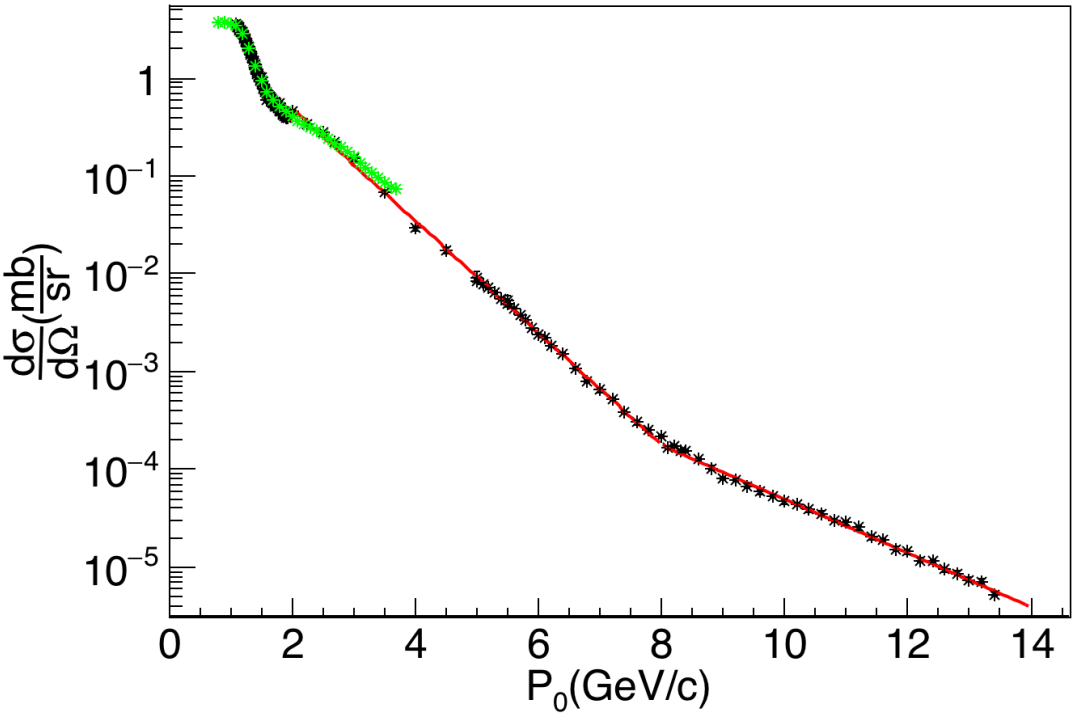

Fig. 34 (color online) Proton-proton quasi-elastic differential cross sections for $\boldsymbol{\theta_{cm} = 90^o}$ **(black data points)** together with the predictions from SAID model (**green points**). Five different empirical fits (**red curves**) are used to fit the data from 1.1–1.2 GeV/c, 1.2–1.6 GeV/c, 1.6–2.0 GeV/c, 2.0–8.0 GeV/c and 8–14 GeV/c. The method of using different empirical fits to describe the pp quasi-elastic differential cross sections in this kinematical region was first used by [2].

Several cuts are applied to the SRC kinematics simulation in order to estimate the measurement rate of A(p,ppn) and A(p,ppp) (i.e. scattering off np-SRC and pp-SRC pairs). Again, we pick co-planar events by requiring the difference of the azimuthal angles of the two forward going protons to be $\Delta\phi_{lab} = 180° \pm 20°$ having laboratory polar angles θ_{lab} from 18° to 30° and $\theta_{cm} = 90° \pm 30°$. We chose hard scattering events by requiring all Mandelstam variables to be ≥ 2 GeV^2 and we made sure that these events are coming from the SRC tail by applying a cut 0.25 (GeV/c) $\leq P_{miss} \leq$ 1.0 (GeV/c) and 0.25 (GeV/c)$\leq P_{recoil} \leq$ 1.0 (GeV/c). A cut was also applied on the polar angle of the backward going recoil nucleon, requiring $115^o \leq \theta_{recoil} \leq 155^o$. A summary of all cuts can be seen in Table 6.

Quantities	**Cuts**
θ_{cm}	$80^o \leq \theta_{cm} \leq 100^o$
θ_{lab} of P_1,P_2	$18° \leq \theta_{lab} \leq 30°$
|s,t,u|	≥ 2 GeV^2
$\Delta\phi_{lab} = \|\phi_1 - \phi_2\|$ of P_1,P_2	$160° \leq \Delta\phi_{lab} \leq 200°$
P_{miss}	0.27 (GeV/c)$\leq P_{miss} \leq$1.0(GeV/c)
P_{recoil}	0.27 (GeV/c)$\leq P_{recoil} \leq$1.0(GeV/c)
θ_{recoil}	$115^o \leq \theta_{recoil} \leq 155^o$

Table 6 A summary of the cuts applied at SRC simulation for the estimation of the measurement rates.

Using the above cuts, the aforementioned assumptions and the pp differential cross sections, we calculated the rate of A(p,ppn) and A(p,ppp) for first SRC measurement (in parallel to the di-lepton run) and for the second SRC measurement (the future dedicated run).

The expected total number of events for the first SRC measurement is:

- **np-SRC via ^{107}Ag(p,2pn): 2,200 events.**

Based on the expected trigger rate from GEANT3 simulation, (~32 kHz see figure 20), the assumed running time (28 days) and the duty cycle (10%), we estimated that a total amount of 7.7×10^9 triggers will be recorded by the HADES detector. Collaboration is aiming towards the goal of recording a total amount of 9.0×10^9 triggers out of which **2,570** (=2,200 x $9.0 \times 10^9 / 7.7 \times 10^9$) will come from SRC events.

For the future dedicated SRC measurement, the expected total number of events is:

- **np-SRC via. A(p,2pn): 10,000 events.**
- **pp-SRC via. A(p,2pp): 1,050 events.**

4.3.2 Background Estimation

To estimate the amount of background events leaking into the expected signal region, we used a simulation using as input events from UrQMD transport code passed through the GEANT3 HADES simulation including NeuLAND. The estimations presented below are based on the analysis of 10^9 p+^{93}Nb background interactions and 5×10^5 SRC events with an incident proton kinetic energy of 4.5 GeV (5.3 GeV/c). The signal and background simulation event samples were scaled appropriately to match the relative rates (in practice, the signal sample was scaled down). Fig. 35 shows the momentum distribution of the recoil neutron together with the background distribution of the neutral particles (neutrons and photons). A cut at $P_{recoil} \geq 0.27$ GeV/c will be applied to ensure the selection of neutrons coming from SRC-pairs. After the cut, a small leakage of background neutral particles is expected into the signal as can be seen in fig. 35. The signal to background ratio is estimated based on the simulation to be 10:1.

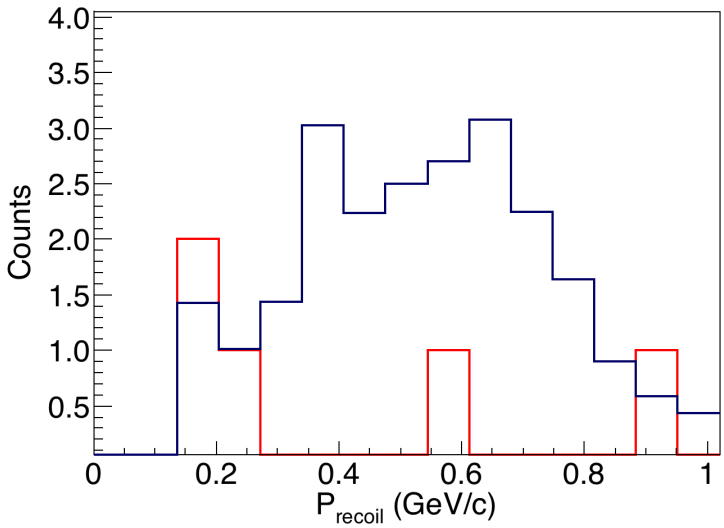

Fig. 35 The momentum distribution of the recoil neutron from SRC pairs in comparison to the background distribution of the neutral particles as estimated based on UrQMD+GEANT3 simulation. A small leakage of background events into the signal region is observed.

4.3.3 NeuLAND Resolution and Efficiency

The first measurement of SRCs using HADES and NeuLAND detectors will take place in parallel to a di-lepton dedicated run. The di-lepton dedicated run will use the full HADES spectrometer including the new RICH detector. The material budget of new RICH detector will not allow us to detect the recoil protons from the SRC pair. The recoil neutrons will be measured with some efficiency, which is the convolution of the intrinsic efficiency of recoil detector (NeuLAND + two side walls) and the multi-scattering due to the materials in the target area—mainly the RICH. A study of recoil detector efficiency and resolutions for neutrons with momenta 0.1-1 GeV/c with and without the new RICH in place was performed by implementing NeuLAND detector and the side walls in the official HADES GEANT3 simulation package. Fig. 36 shows the recoil detector implemented into the main GEANT3 simulation. GEANT3 simulation was updated to include the material of the new RICH.

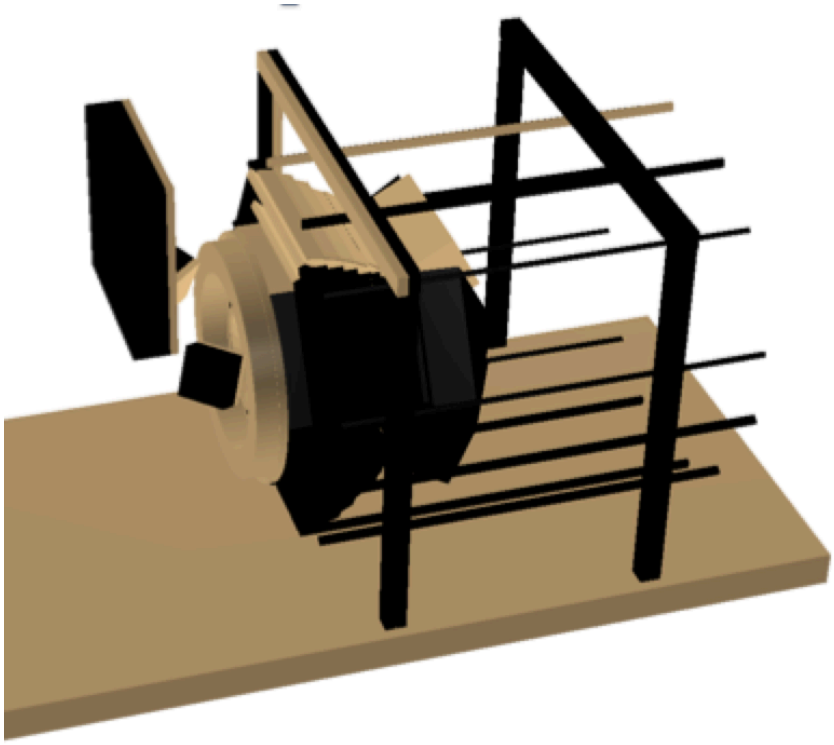

Fig. 36 The NeuLAND detector (6 detection planes with 2.5x2.5x0.1 m^3 dimensions, overall dimensions of 2.5x2.5x0.6 m^3) together with the two small side walls (4 detection planes each with 0.7x0.7x0.1 m^3 dimensions, overall dimensions of 0.7x0.7x0.4 m^3) and the HADES detector with its support structure including the new RICH.

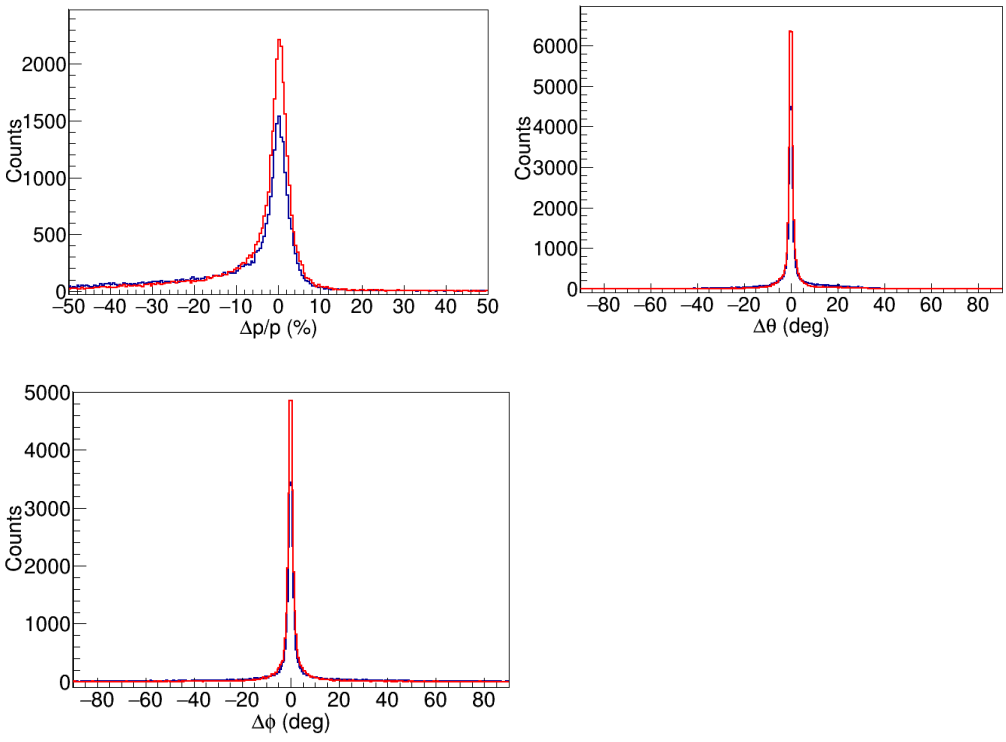

Fig. 37 (Color online) The relative momentum resolution (top left panel), the polar angular resolution (top right panel) and the azimuthal angular resolution

(bottom left panel) as predicted based on a GEANT3 simulation of the NeuLAND and HADES detectors **with** and **without** the new RICH in place.

Based on the GEANT3 simulation, we studied how the new RICH affects the efficiency and the momentum, the polar and azimuthal angular resolutions of the recoil detector. Fig. 37 shows the momentum, polar and angular resolutions with and without the RICH. The RICH has little to almost no effect on the neutron resolutions. This gives us additional confidence that the neutron recoil momentum can be reconstructed accurately and that the Migdal jump can be studied quantitatively for the first time.

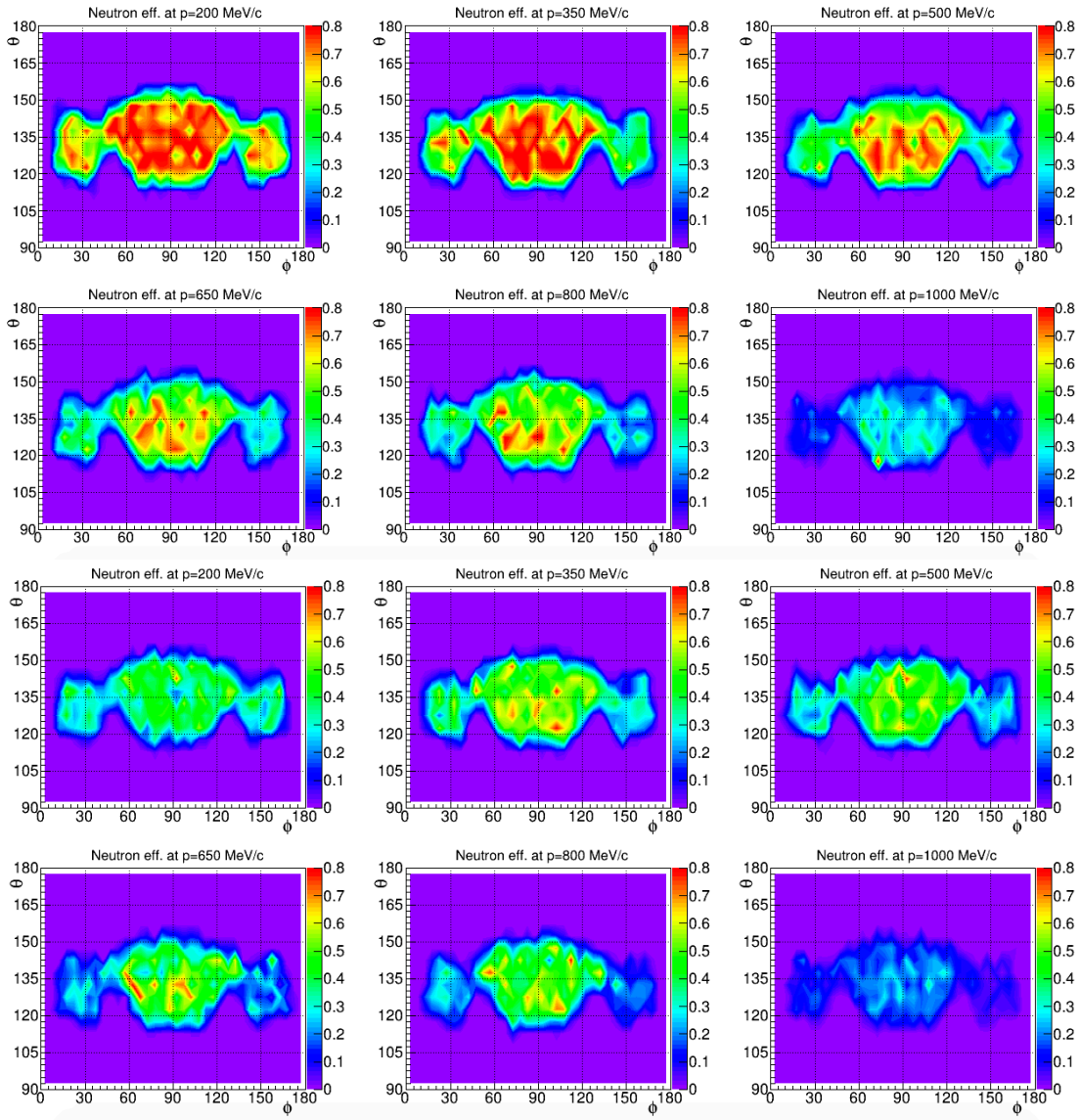

Fig. 38 (color online) The efficiency of NeuLAND (color scale) plotted in the polar-azimuthal angle plane as a function of gradually increasing momentum bins from 200–1000 MeV/c. The top two rows show the efficiency of recoil detector without the new RICH while the bottom two rows show its efficiency for the same momentum bins with the new RICH in position.

The effect of the new RICH material budget on the overall efficiency of recoil detector system detector was studied in detail. Fig. 38 shows the neutron

efficiency (color scale) of recoil detector plotted in the polar-azimuthal angle plane as a function of the incident neutron momentum in bins of $\pm$ 75 MeV/c starting from 200 MeV/c up to 1000 MeV/c. The top two rows show the efficiency of the recoil detector without the presence of RICH while the bottom two rows show its efficiency with RICH in place.

The average efficiency at the center of NeuLAND detector with and without RICH as a function of incident neutron momentum can be seen in Fig. 39. The efficiency varies from ~80% (~55%) at 200 MeV/c to ~60% (~45%) at 1000 MeV/c without (with) RICH in place. An overall ~20% reduction efficiency is observed, which was taken into account at the signal rate estimates.

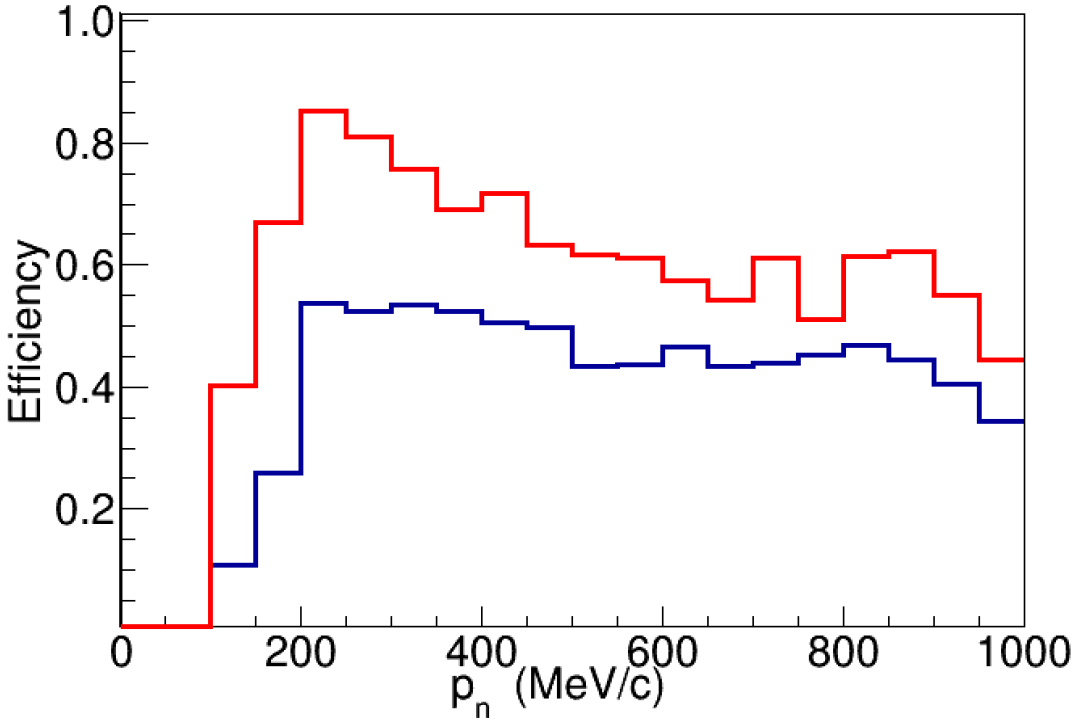

Fig. 39 shows the average efficiency at the center of NeuLAND detector with and without the RICH as a function of incident neutron momentum. An efficiency varying from ~80% at 200 MeV/c to ~60% at 1000 MeV/c is observed without the RICH detector while an efficiency of 55% to 45% is observed in the same momentum region with RICH in place. An overall 20% reduction in efficiency is due to the new RICH.

5. References

[1] R. Subedi *et al.*, Science **320**, 1426 (2008).
[2] O. Hen *et al*., (CLAS Collaboration), Science **346**, 614 (2014).
[3] I. Korover *et al*. (Hall-A Collaboration), Phys. Rev. Lett. **113**, 022501 (2014)
[4] R. Shneor *et al.,* Phys. Rev. Lett. **99**, 072501 (2007),
[5] O. Hen *et al.,* (CLAS Collaboration), Phys. Lett. B **772**, 63 (2013).
[6] K.S. Egiyan *et al.,* Phys. Rev. Lett. **96**, 082501 (2006)
[7] Fomin PRL
[8] K.S. Egiyan *et al.,* Phys. Rev. C 68, 014313 (2003).
[9] C. Colle *et al.,* In-Preparation (2015).
[10] O. Hen *et al.,* In-Preparation (2015).
[11] O. Hen *et al.,* In-Preparation (2015).
[12] M. M. Sargsian *et al.,* PRC 71 044615 (2005).
[13] Ciofi and Alvioli PRL 100, 162503 (2008).
[14] Schiavilla et al., Phys. Rev. Lett. **98**, 132501 (2007).
[15] L. B. Weinstein, E. Piasetzky, D. W. Higinbotham, J. Gomez, O. Hen, and R. Shneor, Phys. Rev. Lett. **106**, 052301 (2011).
[16] O. Hen, E. Piasetzky, and L.B. Weinstein, Phys. Rev. C **85**, 047301 (2012).
[17] O. Hen, D. W. Higinbotham, G. Miller, E. Piasetzky, and L. B. Weinstein, Int. J. Mod. Phys. E **22**, 133017 (2013).
[18] D. W. Higinbotham, G. Miller, O. Hen, and K. Rith. CERN Cour. 53N4, 35 (2013)
[19] L. Frankfurt *et al.,* Int.J.Mod.Phys. A **23** (2008) 2991-3055
[20] O. Hen *et al.,* Phys. Rev. C **91**, 025803 (2015).
[21] M. Martini *et al.,* Phys.Rev. D **85**, 093012 (2012).
[22] G. A. Fiorentini *et al.,* (MINERvA Collaboration), Phys. Rev. Lett. **111**, 022501 (2013); ibid 022502.
[23] O. Hen, L. B. Weinstein, E. Piasetzky, G. A. Miller, M. M. Sargsian, and Y. Sagi, submitted for publication. arXiv: 1407.8175.
[24] A. Tang *et al.,* Phys. Rev. Lett. **90**, 042301 (2003).
[25] E. Piasetzky *et al.,* Phys. Rev. Lett. **97**, 162504 (2006).
[26] D. Higinbotham, E.Piasetzky, M.Strikman "Protons and Neutrons Cosy Up In Nuceli and Neutron Stars", CERN COURIER 49N1:22-24,2009.
[27] L.L. Frankfurt and M.I. Strikman, "Hard nuclear processes and microscopic nuclear structure", Phys. Rep. **160**, 235 (1988).
[28]
[29] J. Arrington, D.W. Higinbotham, G. Rosner, M. Sargsian, "Hard probes of short-range nucleon-nucleon correlations", Progress in Part. and Nucl. Physic, 67, 898 (2012).
[28] L. Frankfurt *et al.,* Phys. Rev. C 48, 2451 (1993).
[29] D. F. Geesaman, K. Saito and A. W. Thomas, "The nuclear EMC effect", Ann. Rev. Nucl. Part. Sci. 45, 337 (1995).
[30] J. L. S. Aclander *et al.,* Phys. Lett. B 453, 211 (1999).
[30] P. R. Norton, "The EMC effect", Reports on Progress in Physics 66, 1253 (2003).
[31] L. Frankfurt and M. Strikman, "Photon parton distributions in nuclei and the EMC effect", Phys. Rev. C 82, 065203 (2010).

[32] O. Hen, L. Weinstein, S. Gilad, and S.A. Wood (spokespersons), JLab Experiment E12-11-107.
[33] G. P. Zeller *et al.,* Phys. Rev. Lett. 88, 091802 (2002).
[34] J. Lattimer and Y. Lim, Astrophys. J. 771, 51 (2013).
[35] E. Braaten, Lect. Notes Phys. 836, 193 (2012).
[36] Stewart *et al.,* PRL 104, 235301 (2010)
[37] C. Colle *et al.,* Phys. Rev. C 89, 024603 (2014).
[38] The R^3B collaboration, Technical Report for the Design, Construction and Commissioning of NeuLAND: The High-Resolution Neutron Time-of-Flight Spectrometer for R^3B, Available at http://www.fair-center.eu/fileadmin/fair/publications_exp/NeuLAND-TDR-Web.pdf [Verified at 01/27/2017]
[39] S. A. Bass et al., Prog. Part. Nucl. Phys. 41, 225-370 (1998).
[40] M. Bleicher et al., J. Phys. G: Nucl. Part. Phys. 25, 1859-1896 (1999).
[41] J. Aclander *et al*., Phys. Rev. C 70, 015208 (2004).
[42] C.W Akerlof *et al.,* Phys. Rev. 159, 1138(1967).
[43] R.C Kammerud *et al.,* Phys. Rev. D 4,1309(1971).
[44] D.Sivers *et al.,* Physics Reports 1, 1-121(1976).
[45] M.Garcon *et al.,* Nuclear Physics A 445, 669(1985).
[46] Institute for Nuclear Studies, The SAID Partial-Wave Analysis Facility, Department of Physics, The George Washington University, Available at http://gwdac.phys.gwu.edu [Verified at 01/27/2017]